Photoinduced transfer hydrogenation of N_2 to NH_3 using a Mo-catalyst and a Hantzsch ester donor is demonstrated with and without an Ir-photoredox co-catalyst

Christian M. Johansen, Emily A. Boyd, Jonas C. Peters*

Affiliations:

Division of Chemistry and Chemical Engineering, California Institute of Technology; Pasadena, CA 91125, USA.

*Corresponding author. Email: jpeters@caltech.edu

Abstract: Whereas photoredox catalysis using molecular systems enjoys considerable utility in small molecule transformations and reactions relevant to organic synthesis, to date there are no related examples of photodriven catalytic nitrogen fixation. We wondered whether a photoinduced transfer hydrogenation strategy might provide a viable pathway toward such a reaction. Hantzsch esters (and related organic structures) offer an opportunity for catalysis design in this context as they can behave as photoreductants, though to our knowledge they had yet to be shown to be compatible with such a redox intensive process (6 e^-/6 H^+). In the present study we demonstrate that fully reduced Hantzsch esters (abbreviated as HEH_2) successively deliver stored H_2-equivalents to N_2, producing NH_3 catalytically, in the presence of a molecular precatalyst (Mo) under blue-light irradiation but otherwise ambient conditions. While not required for the observed photocatalysis, the addition of a photoredox catalyst (Ir) to the reaction mixture enhances both the rate and turnover number of the net transformation. Encouraging with respect to future studies toward recycling the donor, electrochemically or via hydrogenation, other N-heterocycle H_2-donors are also compatible with catalysis in the presence of the photoredox catalyst. The reduction of N_2 to NH_3 by HEH_2 or H_2 are thermodynamically very similar ($\Delta\Delta G_f(NH_3)$ = 1.8 kcal mol^{-1} in acetonitrile). However, whereas the combination of H_2 with N_2 to produce NH_3 is accomplished via high temperature and pressure over a metal catalyst, the needed overpotential to drive the reduction of N_2 by HEH_2 can instead be derived from light. This study hence illustrates a promising photoredox catalysis approach toward deep reduction of robust small molecule substrates via photoinduced transfer hydrogenation, with the complete reduction of the triple bond of N_2 providing a vivid example.

Main Text:

Multi-electron reductive transformations of small molecule substrates (e.g., N_2, CO_2, P_4) are challenging to mediate in homogeneous catalysis and most typically require considerable energy input via harsh chemical reagents and/or conditions to be driven forward. The nitrogen reduction reaction (N_2R) offers a case in point; substantial progress has now been made in molecular catalyst design but significant overpotentials are generally needed to observe NH_3 product.[1,2,3] For N_2R, kinetic challenges also prevail for enzymatic and heterogeneous catalysis that require substantial energy inputs, via ATP hydrolysis for the former and high temperature and pressure or electrochemical overpotential for the latter,[4,5,6] despite a thermally favorable Gibbs free energy of formation, $\Delta G_f(NH_3)$ (Figure 1A).

The organometallic catalysis field has pursued photochemical strategies as a means of driving small molecule reductions, with considerable success being achieved for CO_2 reduction (CO_2R, typically by 2 e^-/2 H^+) as the target transformation.[7,8] Such strategies are still challenged by the widespread use of sacrificial donors whose oxidation products are not readily recycled. While design schemes are envisaged to someday couple photodriven CO_2R catalysis with water oxidation, photodriven transfer hydrogenation using a suitable precatalyst offers an approach to reductive small molecule catalysis, especially if the net H_2-donor (subH_2; Figure 1B) derives from a structure than can be efficiently recycled, for example via hydrogenation or electrochemically.

Fully reduced Hantzsch esters (HEH_2, Figure 1B) and chemically related structures (e.g., reduced acridine, phenanthridine) have been explored for thermally and photochemically driven reductive hydride (H^-; NADH-like) and H-atom transfers in organic synthesis.[9] Moreover, they are highlighted for their chemical (and electrochemical) recyclability via net hydrogenation of the spent pyridine-type oxidation product.[10,11] Whereas the types of transformations they participate in are generally two-electron processes, it is tempting to explore whether they might also be employed for deeper multi-electron reductions of the type pursued in small molecule reductive catalysis. Focusing on N_2R,[12] we noted that despite long known and still debated studies of photocatalytic nitrogen fixation using semiconductors,[13,14,15] and photodriven N_2R mediated by nitrogenase coupled with CdS,[16,17] as yet there are no examples of photochemically driven catalytic N_2R using well-defined molecular systems. Hence, photodriven N_2R via transfer hydrogenation from a Hantzsch ester or related donor, which requires the donors to engage in successive transfers to mediate a deep 6 e^-/6 H^+ reduction process, provides an excellent test case of this strategy.

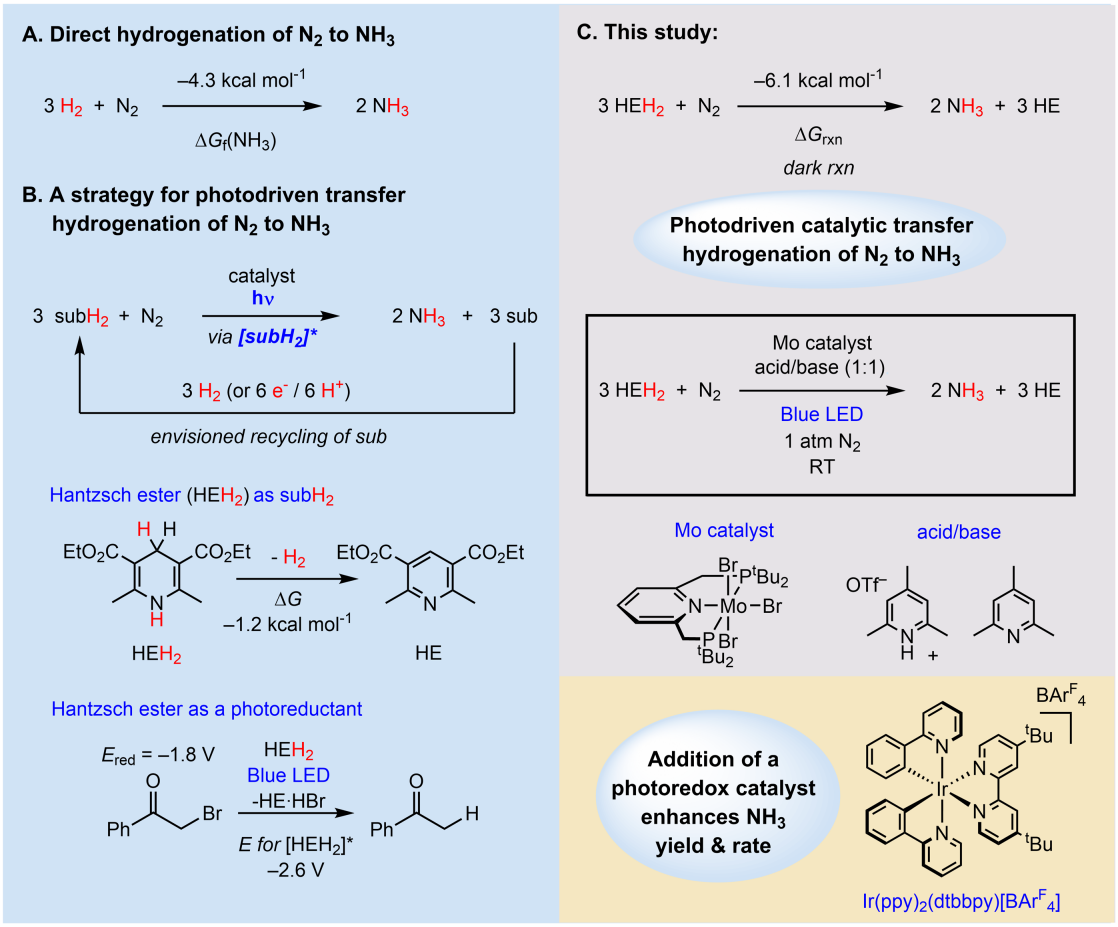

Fig. 1. Thermodynamics and strategies for hydrogenation of N_2. (**A**) Thermodynamics of hydrogenation of N_2 to NH_3; (**B**) Schematic of an overall design for light-driven transfer hydrogenation of N_2; chemical structure of the Hantzsch ester used in this study (HEH_2); representative reduction of α-bromo acetophenone; (**C**) Net stoichiometry and estimated driving force of transfer hydrogenation from HEH_2 to N_2 forming NH_3; photodriven (blue LED) process described in this study, in the absence and presence of a photoredox catalyst. All thermochemical values are given in MeCN at 25 °C with ferrocenium/ferrocene ($Fc^{+/0}$) as reference potential.

Considering thermodynamic parameters relevant to the aforementioned goals, in its ground state the first C–H bond dissociation free energy ($BDFE_{C–H}$) of HEH_2 is 62.3 kcal $mol^{–1}$ in MeCN at 25 °C (all following thermochemical values are defined at these conditions), which is not weak enough to bimolecularly liberate H_2.[18] Photoexcitation of HEH_2, however, renders an excited state that is highly reducing (E_{ox} for $[HEH_2]^*$ is ~ –2.6 V vs $Fc^{+/0}$; Fc = ferrocene).[19,20] Photodriven (blue LED) reduction of α-bromo acetophenone to acetophenone by HEH_2 illustrates its capacity to deliver an H_2 equivalent (Figure 1B).[19] For a dark N_2R reaction, we estimate the overpotential for reduction of N_2 by HEH_2 to generate NH_3 as 1.8 kcal $mol^{–1}$ (($\Delta\Delta G_f(NH_3)$, Figure 1C). Using light (blue LED), we show herein that it is indeed possible to catalyze photoinduced transfer hydrogenation from HEH_2 to N_2 using a known molybdenum pre-catalyst (Figure 1C)[21] at atmospheric pressure and 23 °C. The inclusion of an Ir-photoredox catalyst (Figure 1C) within this system, while not necessary for turnover, enhances the yields and rates of NH_3 generation.

For our present catalysis system, we noted that a photoreduction step from the excited state of HEH_2, $[HEH_2]^*$, liberates the ground state radical cation $HEH_2^{\bullet+}$, which is a sufficiently strong

oxidant (E_{red} = 0.48 V vs $Fc^{+/0}$) to be deleterious to N_2R.[18] We therefore reasoned that inclusion of a base to deprotonate $HEH_2^{\bullet+}$ ($pK_a \sim -1$) would be prudent.[18] However, the presence of a moderate Brønsted acid is typically required for chemically driven N_2R, suggesting a buffered system might be needed. A collidine/collidinium (abbreviated Col/[ColH]$^+$; Col = 2,4,6-trimethylpyridine) mixture was chosen as Col will readily deprotonate $HEH_2^{\bullet+}$ while [ColH]$^+$, with a pK_a of 15 in MeCN,[22] has been shown to be compatible with chemically driven N_2R by Nishibayashi and coworkers using (PNP)$MoBr_3$ as a pre-catalyst (PNP = 2,6-bis(di-tert-butylphosphinomethyl)pyridine) with $(Cp^*)_2Co$ ($E_{1/2}(Co^{III/II})$ = −1.91 V; Cp* = pentamethylcyclopentadienyl) as the reductant.[21,23]

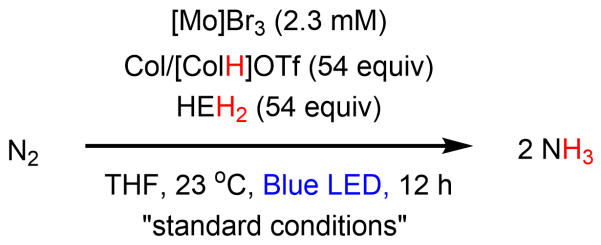

Entry	Change from "standard conditions"	NH_3 (equiv/ Mo)	NH_3 yield/ HEH_2 (%)
1	none	9.5 ± 1	26.5 ± 3
2	0.57 mM $[Mo]Br_3$	21.8 ± 0.8	15.1 ± 0.6
3	No light	<0.1	<0.3
4	No buffer	0.9 ± 0.2	2.6 ± 0.5
5	5 equiv Col/[ColH]OTf	2.9 ± 0.2	8.0 ± 0.6
6	benzene instead of THF	4.7 ± 0.1	13 ± 0.3
7	216 equiv Col/[ColH]OTf	20.3 ± 1.1	56 ± 3
8	10 equiv TBABr	8.8 ± 0.3	23.6 ± 0.8
9	with $[Ir]BAr^F_4$	24 ± 4	67 ± 10
10	with $[Ir]BAr^F_4$, 5 equiv Col/[ColH]OTf	15.8 ± 0.8	44 ± 2
11	with $[Ir]BAr^F_4$, t = 1/2 h instead of 12 h	18.6 ± 0.9	52 ± 3
12	t = 2 h instead of 12 h	7.6 ± 2	21 ± 6
13	with $[Ir]BAr^F_4$, 5 equiv Col/[ColH]OTf, 0.57 mM $[Mo]Br_3$	26 ± 0.4	18.4 ± 0.4
14	with $[Ir]BAr^F_4$, 5 equiv Col/[ColH]OTf, no light	<0.1	<0.3
15	with $[Ir]BAr^F_4$, 5 equiv Col/[ColH]OTf, no $[Mo]Br_3$	<0.1	<0.3
16	with $[Ir]BAr^F_4$, 5 equiv Col/[ColH]OTf, no HEH_2	<0.1	<0.3
17	with $[Ir]BAr^F_4$, $subH_2$ = 9,10-dihydroacridine	6.4 ± 0.3	17.7 ± 0.8
18	with $[Ir]BAr^F_4$, $subH_2$ = 5,6-dihydrophenanthridine	4.6 ± 0.8	13 ± 2
19	with $[Ir]BAr^F_4$, $subH_2$ = 1-benzyl-1,4-dihydronicotinamide	1.2 ± 0.1	3.3 ± 0.3
20	with $[Ir]BAr^F_4$, 0.5 atm H_2, 0.5 atm N_2	14 ± 4	36 ± 9
21	with $[Ir]BAr^F_4$, no Col/[ColH]OTf	7.4 ± 0.4	20.7 ± 1

Table 1. Catalytic yields for photodriven transfer hydrogenation of N_2 to NH_3. Reactions performed with 2.3 mM $[Mo]Br_3$ concentration, using a single 34 W Kessel H150 Blue lamp unless otherwise noted. All NH_3 yields reported are an average of at least two runs. All runs with $[Ir]BAr^F_4$ used 2.3 mM photosensitizer loading.

We find that $[Mo]Br_3$ (1 equiv at 2.3 mM) in the presence of 54 equiv each of HEH_2, [ColH]OTf (OTf = triflate), and Col in THF, under an N_2 atmosphere and blue LED irradiation at 23 °C for 12 hours, yields 9.5 ± 1 equiv NH_3/Mo (Table 1, entry 1). Assuming HEH_2 is a 2 e^- donor in this process provides an NH_3 yield with respect to HEH_2 of ~25%. Use of $^{15}N_2$ confirmed N_2 as the source of the NH_3 produced (Figure S2). To cement this interpretation, using either ^{15}N-labeled HEH_2 or ^{15}N-labeled Col/[ColH]OTf produced only $^{14}NH_3$. Analysis of the organic

products following catalysis revealed complete consumption of HEH_2, with the fully oxidized Hantzsch ester pyridine (HE) as the major organic biproduct, consistent with HEH_2 acting as a 2 e^-/2 H^+ donor. We note that the yield of HE is ~80%; similarly, ~20% of the initial buffer loading is not recovered (Figure S7). One possibility is the light-induced parasitic reductive coupling of pyridines (either Col or HE), as has been previously observed with HE.[24] Also, one factor limiting NH_3 selectivity per HEH_2 concerns background hydrogen evolution under blue light irradiation (see Figure S8).

Higher yields of NH_3 per Mo center could be obtained by decreasing the $[Mo]Br_3$ loading (21.8 ± 0.8 equiv/Mo; entry 2), but with a loss in the yield of NH_3 with respect to HEH_2. Irradiation was required to generate NH_3, and yields were substantially lower without the added buffer (entries 3-4). Attempts to use catalytic amounts of Col/[ColH]OTf (5 equiv per $[Mo]Br_3$) substantially lowered the NH_3 yields (entry 5). The reaction run in benzene instead of THF gave attenuated yields (4.7 ± 0.1 equiv NH_3/Mo; entry 6) but remained catalytic.

While future studies are needed to probe the mechanism of this transformation, the fate of photoexcited $[HEH_2]^*$ is likely key. Two limiting scenarios to consider are the direct reduction of N_2R intermediates by $[HEH_2]^*$ (Figure 2A), or the reduction of the [ColH]OTf to $[ColH]^\bullet$ radical, which then reacts with $M(N_2)$ (Figure 2B) to form an N–H bond via $M(N_2H)$. Pyridyl radicals have been posited as possible intermediates of N_2R in thermally driven catalysis with molecular systems.[25] Figures 2A and 2B are generalized representations to help illustrate how a photon can facilitate delivery of H_2 from HEH_2 to $M(N_2)$ to first generate $M(NNH_2)$ and ultimately NH_3. While for simplicity we depict this first conversion to $M(NNH_2)$, various scenarios, for example via generation and then reduction of a terminal nitride intermediate ($Mo{\equiv}N + HEH_2 \rightarrow Mo(NH_2) + HE$), also warrant consideration.[26] A recent study showed that a $Mn^V{\equiv}N$ can be photoreduced by 9,10-dihydroacridine to liberate NH_3.[27]

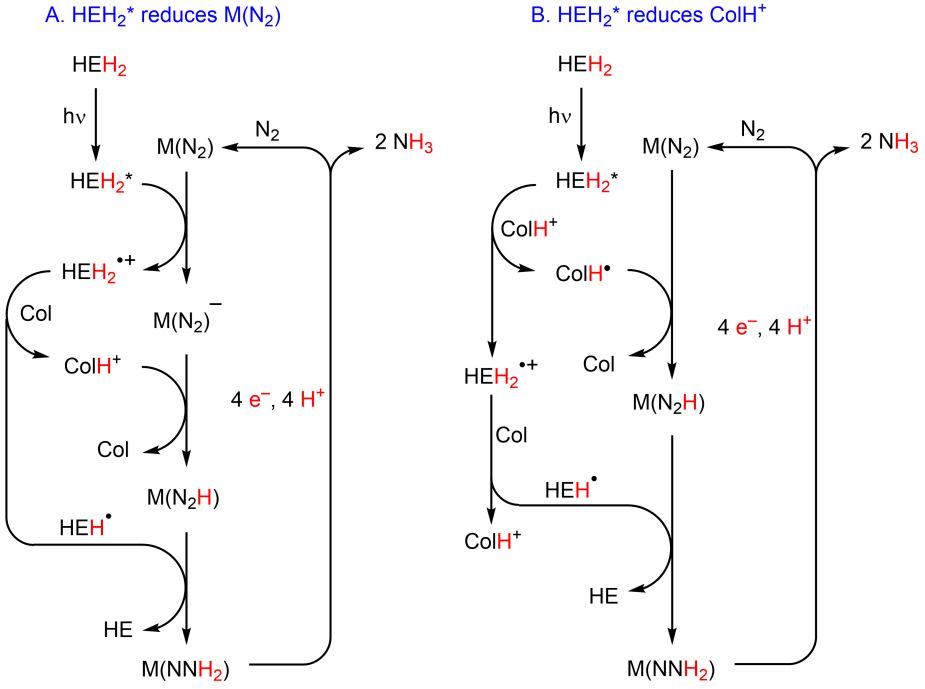

Fig. 2. Possible scenarios rationalizing photodriven transfer hydrogenation from HEH_2 to N_2 mediated by a metal catalyst and buffer system (Col/$[ColH]^+$). (**A**) Scenario in which $[HEH_2]^*$

is oxidatively quenched by a metal-bound N_2R intermediate; (**B**) Scenario in which $[HEH_2]^*$ is oxidatively quenched by $[ColH]^+$ to generate $[ColH]^{\bullet}$.

Increasing the buffer concentration to 216 equiv/Mo boosted the NH_3 yield to 20.3 ± 1.1 equiv NH_3/Mo (entry 7). This observation points to a pathway whereby reduction of [ColH]OTf by $[HEH_2]^*$ dominates (Figure 2B), consistent with the high reactivity expected of $[HEH_2]^*$ (E_{ox} ~ –2.6 V; pK_a ~ –20; $BDFE_{C–H}$ ~ –8.5 kcal $mol^{–1}$), as well as its short solution lifetime (0.419 ns in DMSO solvent at 25 °C).[18,20] Accordingly, steady state-fluorimetry studies show efficient quenching of $[HEH_2]^*$ upon titrating in [ColH]OTf (Figure S9). However, as some NH_3 can be detected under irradiation even in the absence of buffer (entry 4), other photoinduced pathways for N–H bond formation via HEH_2 are clearly accessible. The addition of 10 equiv of tetrabutylammonium bromide (TBABr) had no effect on the NH_3 yield (entry 8), suggesting that reductive $Br^–$ loss from the precatalyst is not a limiting factor.

Limitations stemming from a short $[HEH_2]^*$ excited-state lifetime and low quantum yield (0.031)[20] for HEH_2 motivated us to explore a photosensitizer to enhance this photodriven catalysis. To test this idea, $[Ir(ppy)_2(dtbbpy)]BAr^F_4$ ($[Ir]BAr^F_4$, ppy = 2-phenylpyridinyl, dtbbpy = 4,4′-di-tert-butyl-2,2′-bipyridine; BAr^F_4 = tetrakis(3,5-bis(trifluoromethyl)phenyl)borate; $E_{1/2}(Ir^{III/II})$ = −1.90 V) was chosen as its reduction potential is close to that of Cp^*_2Co and hence should be compatible with N_2R using $[Mo]Br_3$.[28,21]

Including $[Ir]BAr^F_4$ with $[Mo]Br_3$ (1 equiv, both at 2.3 mM), in addition to 54 equiv each of HEH_2 and Col/[ColH]OTf in THF, under an N_2 atmosphere and blue LED irradiation for 12 hours at room temperature, yielded 24 ± 4 equiv of NH_3/Mo (entry 9). Assuming HEH_2 is a 2 $e^–$/2 H^+ donor, these conditions correspond to an overall NH_3 yield of 67 ± 10% with respect to HEH_2. Furthermore, in the presence of the Ir photosensitizer, catalytic amounts of buffer can be used, producing 15.8 ± 0.8 equiv NH_3/Mo (entry 10). In addition to higher yields, the inclusion of $[Ir]BAr^F_4$ enhances the photocatalytic rate; the catalysis is ~80% complete after 30 minutes (entry 11). By contrast, under Ir-free conditions, 2 hour reaction times are required to achieve ~80% completion (entry 12).

As in the Ir-free process, lowering the $[Mo]Br_3$ loading increased turnover for NH_3 with catalytic buffer (26.0 ± 0.4 equiv NH_3/Mo, entry 13), but with decreased selectivity. No NH_3 is produced without irradiation (entry 14), and the presence of $[Mo]Br_3$ and HEH_2 are likewise essential (entries 15-16). Similar to the Ir-free reaction, HE was found to be the major organic product (>80%) and complete consumption of HEH_2 was observed (Figure S4). Solvent screening suggests that the reaction is most efficient when all components are soluble (see Table S5). By contrast, other catalytic N_2R methods rely on low solubility of either the acid or reductant to attenuate competing H_2 evolution, demonstrating an advantage to using a terminal H-atom source which is not competent for H_2 release in the ground state.[1]

A range of candidate H_2 carriers, subH_2, should be explored in future studies to identify donors whose spent products can be recycled efficiently, perhaps *in situ*, via hydrogenation with H_2 or electrochemically (2 $e^–$/2 H^+). The Ir-photosensitizer cocatalyst enables catalytic production of NH_3 under irradiation with 9,10-dihydroacridine or 5,6-dihydrophenanthridine as the H_2 donor (6.4 ± 0.3 equiv NH_3/Mo and 4.6 ± 0.8 equiv NH_3/Mo, respectively, entries 17-18). While non-catalytic, N_2-to-NH_3 conversion is also achieved with [Ir] and the hydride donor 1-benzyl-1,4-dihydronicotinamide (1.2 ± 0.1 equiv NH_3/Mo, entry 19). In the absence of [Ir], none of these H_2 or $H^–$ carriers are competent for the photoinduced N_2RR (see Table S2). The reaction with HEH_2 tolerates a 1:1 mixture of N_2 and H_2 (1 atm total pressure, 14 ± 4 equiv NH_3/Mo, entry 20),

indicating that the Mo-catalyst is not (at least irreversibly) poisoned by H_2 under these conditions, important for considering downstream recycling of the spent donor.

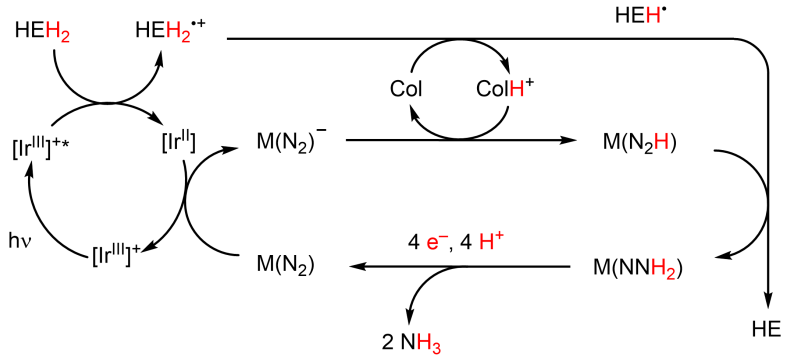

Fig. 3. One possible pathway for photocatalytic reduction of N_2 by HEH_2 upon inclusion of an [Ir]-photosensitizer.

Figure 3 provides a working model to account for the role of [Ir]$BAr^F{}_4$. Upon excitation of $[Ir^{III}]^+$ to $[Ir^{III}]^+$*, reductive quenching by HEH_2 would generate $[Ir^{II}]$, as has been established in related reductions of organic substrates (Figure 3).[9] The resulting radical cation $HEH_2^{\bullet+}$ is then deprotonated by Col, mitigating back-electron transfer from $[Ir^{II}]$. As noted above, $[Ir^{II}]$ is assumed to be sufficiently reducing to generate an $M(N_2)^-$ species from $M(N_2)$. The former would then undergo protonation by $[ColH]^+$ to form an N-H bond via $M(N_2H)$, which itself can be reduced further by diffusing $HEH^\bullet$ to generate $M(NNH_2)$. As noted for Figure 2, this series of steps is plausible but is only one of several related scenarios that may be viable (e.g., $[Ir^{II}]$ might be oxidized by $[ColH]^+$ instead of a [Mo]-species) and future mechanistic studies are needed.

In contrast to the Ir-free conditions, the system with the photosensitizer remains catalytically competent even without added buffer, albeit with an attenuation in turnover (7.4 ± 0.4 equiv NH_3/Mo, entry 21). Presumably, under a Col/$[ColH]^+$-free cycle, the liberated radical cation $HEH_2^{\bullet+}$ (formed via reductive quenching) can be consumed via proton or H-atom transfer with a $[Mo]N_xH_y$ intermediate.

Reagent strengths			$BDFE_{eff}$	$\Delta\Delta G_f$ (NH_3)
HEH_2 BDFE 62.3 kcal mol^{-1}	+	$HEH^\bullet$ BDFE 40.5 kcal mol^{-1}	51.4 kcal mol^{-1}	1.8 kcal mol^{-1}
$[HEH_2]^*$ E_{ox} −2.7 V	+	$ColH^+$ pK_a 15	10.9 kcal mol^{-1}	123 kcal mol^{-1}
$Ir^{II}(ppy)_2(dtbbpy)$ E_{ox} −1.9 V	+	$ColH^+$ pK_a 15	29.3 kcal mol^{-1}	68 kcal mol^{-1}

$$BDFE_{Eff} = 23.06(E_{ox}) + 1.37(pK_a) + C_G \quad (1)$$

$$\Delta\Delta G_f(NH_3) = 3((BDFE_{H2})/2 - BDFE_{Eff}) \quad (2)$$

Fig. 4. Estimated $BDFE_{eff}$ values and corresponding $\Delta\Delta G_f(NH_3)$ for the transformations of interest herein. Values estimated using eqns 1 and 2.

It is interesting to further consider the thermodynamics of both the photodriven N_2R system described here and its hypothetical dark reaction (Figure 1C). To do this one can compare the $BDFE_{eff}$ (Figure 4, eqn 1), a measure of the thermodynamics of H-atom transfer from a set of reagents, to the BDFE of H_2 (103.9 kcal mol^{-1}).[29,30,31] The difference between these values provides an overpotential for N_2 hydrogenation, expressed as $\Delta\Delta G_f(NH_3)$ (eqn 2).[32] For the dark reaction, the $BDFE_{eff}$ is the average of the first (C−H) and second (N−H) BDFE's for HEH_2 and $HEH^{\bullet}$, respectively, correlating to a very small overpotential ($\Delta\Delta G_f(NH_3)$ = 1.8 kcal mol^{-1}).[18] NH_3 synthesis via transfer hydrogenation from HEH_2 to N_2 is therefore thermodynamically comparable to N_2 hydrogenation by the Haber-Bosch process. Where the latter uses high temperature and pressure to overcome the high kinetic barrier, the photodriven process described here obtains excess driving force directly from visible light. More specifically, under conditions that exclude the photosensitizer, using the estimated excited-state reduction potential of $[HEH_2]^*$ and the pK_a of $[ColH]^+$ to estimate $BDFE_{eff}$, blue light affords access to a large added driving force ($\Delta\Delta G_f(NH_3)$ = 123 kcal mol^{-1}; Figure 4) to push the transfer hydrogenation forward. In the presence of the Ir-photosensitizer, a smaller but still significant driving force ($\Delta\Delta G_f(NH_3)$ = 68 kcal mol^{-1}) is available. Regardless, the key point is that light generates an overpotential from an otherwise unreactive source of 2 e^-/2 H^+ stored within HEH_2 that is sufficient to perform, via successive transfers, a net 6 e^-/6 H^+ reduction of N_2 in the presence of an appropriate catalyst and cocatalyst buffer, with additional benefit gained from inclusion of a photoredox co-catalyst. We anticipate that related photodriven transfer hydrogenations of small molecule substrates will prove interesting. Important future goals for the work presented here include extensive mechanistic studies as well as studies aimed at *in situ* recycling of the spent HE back to HEH_2.

References and Notes

[1] M. J. Chalkley, M. W. Drover, J. C. Peters, Catalytic N_2-to-NH_3 (or -N_2H_4) conversion by well-defined molecular coordination complexes. *Chem. Rev*. **120**, 5582–5636 (2020).

[2] Y. Nishibayashi, Development of catalytic nitrogen fixation using transition metal–dinitrogen complexes under mild reaction conditions. *Dalton Trans*. **47**, 11290–11297 (2018).

[3] R. R. Schrock, Catalytic reduction of dinitrogen to ammonia by molybdenum: theory versus experiment. *Angew. Chem. Int. Ed*. **47**, 5512–5522 (2008).

[4] L. C. Seefeldt, B. M. Hoffman, J. W. Peters, S. Raugei, D. N. Beratan, E. Antony, D. R. Dean, Energy transduction in Nitrogenase. *Acc. Chem. Res*. **51**, 2179–2186 (2018).

[5] V. Smil, *Enriching the Earth: Fritz Haber, Carl Bosch, and the Transformation of World Food Production* (MIT Press, Cambridge, MA, 2000).

[6] T. Shima, S. Hu, G. Luo, X. Kang, Y. Luo, Z. Hou, Dinitrogen cleavage and hydrogenation by a trinuclear titanium polyhydride complex. *Science* **340**, 1549–1552 (2013).

[7] Y. Yamazaki, H. Takeda, O. Ishitani, Photocatalytic reduction of CO_2 using metal complexes. *J. Photochem. Photobiol. C: Photochem. Rev.* **25**, 106–137 (2015).

[8] N. Elgrishi, M. B. Chambers, X. Wang, M. Fontecave, Molecular polypyridine-based metal complexes as catalysts for the reduction of CO_2. *Chem. Soc. Rev*. **46**, 761–796 (2017).

[9] P.-Z. Wang, J.-R. Chen, W.-J. Xiao, Hantzsch esters: an emerging versatile class of reagents in photoredox catalyzed organic synthesis. *Org. Biomol. Chem*. **17**, 6936–6951 (2019).

[10] Q.-A. Chen, M.-W. Chen, C.-B. Yu, L. Shi, D.-S. Wang, Y. Yang, Y.-G. Zhou, Biomimetic asymmetric hydrogenation: in situ regenerable Hantzsch esters for asymmetric hydrogenation of benzoxazinones. *J. Am. Chem. Soc*. **133**, 16432–16435 (2011).

[11] G.M. Abou-Elenein, N. A. Ismail, Z. F. Mohammed, H. M. Fahmy, Electroreduction of 2,6-dimethyl-3,4,5-trisubstituted pyridine derivatives in aqueous buffered media at carbon electrode. *Egypt. J. Pharmaceutical Sci*. **33**, 953–962 (1992).

[12] B. M. Comer, P. Fuentes, C. O. Dimkpa, Y.-H. Liu, C. A. Fernandez, P. Arora, M. Realff, U. Singh, M. C. Hatzell, A. J. Medford, Prospects and challenges for solar fertilizers. *Joule* **3**, 1578–1605 (2019).

[13] G. N. Schrauzer, T. D. Guth, Photolysis of water and photoreduction of nitrogen on titanium dioxide. *J. Am. Chem. Soc*. **99**, 7189–7193 (1977).

[14] J. G. Edwards, J. A. Davies, D. L. Boucher, A. Mennad, An opinion on the heterogeneous photoreactions of N_2 with H_2O. *Angew. Chem. Int. Ed*. **31**, 480–482 (1992).

[15] A. J. Medford, M. C. Hatzell, Photon-driven nitrogen fixation: current progress, thermodynamic considerations, and future outlook. *ACS Catal.* **7**, 2624–2643 (2017).

[16] K. A. Brown, D. F. Harris, M. B. Wilker, A. Rasmussen, N. Khadka, H. Hamby, S. Keable, G. Dukovic, J. W. Peters, L. C. Seefeldt, P. W. King, Light-driven dinitrogen reduction catalyzed by a CdS:nitrogenase MoFe protein biohybrid. *Science* **352**, 448–450 (2016).

[17] K. A. Brown, J. Ruzicka, H. Kallas, B. Chica, D. W. Mulder, J. W. Peters, L. C. Seefeldt, G. Dukovic, P. W. King, Excitation-rate determines product stoichiometry in photochemical ammonia production by CdS quantum dot-nitrogenase MoFe protein complexes. *ACS Catal*. **10**, 11147–11152 (2020).

[18] G.-B. Shen, Y.-H. Fu, X.-Q. Zhu, Thermodynamic network cards of Hantzsch ester, benzothiazoline, and dihydrophenanthridine releasing two hydrogen atoms or ions on 20 elementary steps. *J. Org. Chem*. **85**, 12535–12543 (2020).

[19] J. Jung, J. Kim, G. Park, Y. You, E. J. Cho, Selective debromination and α-hydroxylation of α-bromo ketones Using Hantzsch esters as photoreductants. *Adv. Synth. Catal*. **358**, 74–80 (2016)

[20] D.-L. Zhu, Q. Wu, H.-Y. Li, H.-X. Li, J.-P. Lang, Hantzsch ester as a visible-light photoredox catalyst for transition-metal-free coupling of arylhalides and arylsulfinates. *Chem. – Eur. J*. **26**, 3484–3488 (2020)

[21] K. Arashiba, A. Eizawa, H. Tanaka, K. Nakajima, K. Yoshizawa, Y. Nishibayashi, Catalytic nitrogen fixation via direct cleavage of nitrogen–nitrogen triple bond of molecular dinitrogen under ambient reaction conditions. *Bull. Chem. Soc. Jpn*. **90**, 1111–1118 (2017).

[22] S. Tshepelevitsh, A. Kütt, M. Lõkov, I. Kaljurand, J. Saame, A. Heering, P. G. Plieger, R. Vianello, I. Leito, On the basicity of organic bases in different media. *Eur. J. Org. Chem*. **2019**, 6735–6748 (2019).

[23] N. G. Connelly, W. E. Geiger, Chemical redox agents for organometallic chemistry. *Chem. Rev*. **96**, 877–910 (1996).

[24] K. Kano, T. Matsuo, Photoinduced one-electron reduction of 1-benzyl-3-carbamoylpyridinium chloride and 3,5-bis(ethoxycarbonyl)-2,6-dimethylpyridine. *Bull. Chem. Soc. Jpn.* **49**, 3269–3273 (1976).

[25] T. Munisamy, R. R. Schrock, An electrochemical investigation of intermediates and processes involved in the catalytic reduction of dinitrogen by [HIPTN$_3$N]Mo (HIPTN$_3$N = (3,5-(2,4,6-i-Pr$_3$C$_6$H$_2$)$_2$C$_6$H$_3$NCH$_2$CH$_2$)$_3$N). *Dalton Trans*. **41**, 130–137 (2011).

[26] H. Tanaka, K. Arashiba, S. Kuriyama, A. Sasada, K. Nakajima, K. Yoshizawa, Y. Nishibayashi, Unique behaviour of dinitrogen-bridged dimolybdenum complexes bearing pincer ligand towards catalytic formation of ammonia. *Nature Commun*. **5**, 3737–3787 (2014).

[27] D. Wang, F. Loose, P. J. Chirik, R. R. Knowles, N–H bond formation in a manganese(V) nitride yields ammonia by light-driven proton-coupled electron transfer. *J. Am. Chem. Soc*. **141**, 4795–4799 (2019).

[28] J. D. Slinker, A. A. Gorodetsky, M. S. Lowry, J. Wang, S. Parker, R. Rohl, S. Bernhard, G. G. Malliaras, Efficient yellow electroluminescence from a single layer of a cyclometalated iridium complex. *J. Am. Chem. Soc*. **126**, 2763–2767 (2004).

[29] F. G. Bordwell, J. P. Cheng, J. A. Harrelson, Homolytic bond dissociation energies in solution from equilibrium acidity and electrochemical data. *J. Am. Chem. Soc*. **110**, 1229–1231 (1988).

[30] M. Tilset, V. D. Parker, Solution homolytic bond dissociation energies of organotransition-metal hydrides. *J. Am. Chem. Soc*. **111**, 6711–6717 (1989).

[31] R. G. Agarwal, S. C. Coste, B. D. Groff, A. M. Heuer, H. Noh, G. A. Parada, C. F. Wise, E. M. Nichols, J. J. Warren, J. M. Mayer, Free energies of proton-coupled electron transfer reagents and their applications. *Chem. Rev*. **122**, 1–49 (2022).

[32] M. J. Chalkley, J. C. Peters, Relating N–H bond strengths to the overpotential for catalytic nitrogen fixation. *Eur. J. Inorg. Chem*. **2020**, 1353–1357 (2020).

Acknowledgments: We thank the Dow Next Generation Educator Fund and Instrumentation Grants for their support of the NMR facility at Caltech. The Beckman Institute Laser Resource Center and Jay R. Winkler are acknowledged for providing support with steady-state luminescence experiments. We also thank the Resnick Sustainability Institute Water and Environment Laboratory (WEL) at Caltech for the use of their instrumentation.

Funding:

National Institutes of Health (R01 GM-075757)

EAB acknowledges the support of the National Science Foundation for a Graduate Research Fellowship under Grant No. DGE-1745301

Competing interests: Authors declare that they have no competing interests.

Data and materials availability: All data are available in the main text or the supporting information.

Supporting Information

Photoinduced transfer hydrogenation of N_2 to NH_3 using a Mo-catalyst and Hantzsch ester donor is demonstrated with and without an Ir-photoredox catalyst

Christian M. Johansen, Emily A. Boyd, and Jonas C. Peters*

Correspondence to: jpeters@caltech.edu

Figs. S1 to S15
Tables S1 to S6

Table of Contents:

3	S1. Materials and Methods
4	S2. Synthetic details
5-15	S3. Ammonia production and quantification studies
16-21	S4. Analysis of non-NH_3 catalysis products
22-23	S5. Steady-state fluorescence measurements
24	S6. UV-Vis measurements
25-28	S7. Derivation of thermodynamic values
29	S8. NMR spectra

S1. Materials and Methods

S1.1 General Considerations:

All manipulations were carried out using standard Schlenk or glovebox techniques under an N_2 atmosphere. Solvents were deoxygenated and dried by thoroughly sparging with N_2 followed by passage through an activated alumina column in a solvent purification system by SG Water, USA LLC. Nonhalogenated solvents were tested with sodium benzophenone ketyl in tetrahydrofuran (THF) to confirm the absence of oxygen and water. Deuterated solvents were purchased from Cambridge Isotope Laboratories, Inc., degassed, and dried over activated 3-Å molecular sieves prior to use.

HEH_2,[1] $PNPMoBr_3$,[2] [ColH]OTf,[2] BTH_2,[3] $NaBAr^F{}_4$,[4] ^{15}N-Col,[5] $phenH_2$,[6] and $phenazH_2$[7] were prepared according to literature procedures. Triflic acid, ethylacetoacetate, and 37% aqueous formaldehyde were purchased from Sigma Aldrich and used without further purification. $Ir(ppy)_3$ and $Ir(ppy)_2(dtbbpy)[PF_6]$ were purchased from Strem and used without further purification. $^{15}N_2$ was obtained from Cambridge Isotope Laboratories, Inc. (Lot number: I-25854/XZ732957). $^{15}NH_4Cl$ (99% ^{15}N, 98% purity) was purchased from Cambridge Isotope Laboratories, Inc. and used without further purification. Collidine was purchased from Sigma Aldrich and was distilled prior to use. 9,10-dihydroacridine (98%) was purchased from Combi Blocks and used without further purification. Tetrahydrofuran (THF) used in the experiments herein was stirred over Na/K ($\geq$ 12 hours) and filtered over activated alumina or vacuum-transferred before use unless otherwise stated.

Photoinduced reactions were performed using Kessil® 34 W 150 Blue lamps.

S1.2 Physical Methods

NMR: Nuclear Magnetic Resonance (NMR) measurements were recorded with a Varian 400 MHz spectrometer. ^{1}H NMR chemical shifts are reported in ppm relative to tetramethylsilane, using ^{1}H resonances from residual solvent as internal standards.[8]

UV-Vis: Ultraviolet-visible (UV-vis) absorption spectroscopy measurements were collected with a Cary 50 UV-vis spectrophotometer using a 1 cm path length quartz cuvette. All samples had a blank sample background subtraction applied.

EPR Spectroscopy: All X-band continuous-wave electron paramagnetic resonance (CW-EPR) spectra were obtained on a Bruker EMX spectrometer using a quartz liquid nitrogen immersion dewar on solutions prepared as frozen glasses in 2-MeTHF, unless otherwise noted.

Steady-state fluorimetry. Steady-state fluorimetry was performed in the Beckman Institute Laser Resource Center (BILRC; California Institute of Technology). Samples for luminescence measurements were prepared in dry THF and transferred to a 1-cm pathlength fused quartz cuvette sealed with a high-vacuum Teflon valve (Kontes). Steady-state emission spectra were collected on a Jobin S4 Yvon Spec Fluorolog-3-11 with a Hamamatsu R928P photomultiplier tube detector with photon counting.

S2. Synthetic details

S2.1. *Synthesis of ^{15}N-labelled 2,6-Dimethyl-3,5-dicarboethoxy-l,4-dihydropyridine (^{15}N-HEH$_2$).* Adapted from ref 1. Aqueous formaldehyde (37%, 78 μL) and ethylacetoacetate (280 μL, 2.19 mmol) were placed in a 10 mL round-bottom flask equipped with a stir bar and fitted with a reflux condenser. $^{15}NH_4Cl$ (305 mg, 5.7 mmol) in 1 mL H_2O was added to a 1 mL aqueous solution of NaOH (228.3 mg, 5.7 mmol). The resulting solution of $^{15}NH_4OH$ was added to the flask through the neck of the condenser. The condenser neck was rinsed into the flask with 0.5 mL ethanol. The reaction mixture was heated at reflux for 1.5 hrs and then chilled in an ice bath. The resulting precipitate was collected by filtration and washed with cold ethanol (~3 mL) and Et_2O to yield the title compound as a pale yellow powder (60 mg, 22% yield). ^{1}H NMR (400 MHz, DMSO-d_6) δ 8.28 (d, $^1J_{H,N}$ = 94.6 Hz, 1H), 4.05 (q, J = 7.1 Hz, 4H), 3.11 (s, 2H), 2.11 (d, J = 2.9 Hz, 6H), 1.19 (t, J = 7.1 Hz, 6H) ppm.

S2.2 *Synthesis of ^{15}N-labelled 2,4,6-Dimethylpyridinium (^{15}N-[ColH]OTf).* Identical procedure to what has previously been reported with unlabeled Col was employed.[2] ^{1}H NMR (400 MHz, DMSO-d_6) δ 14.87 (broad s, 1H), 7.57 (d, $^3J_{H,N}$ = 2.8 Hz, 2H), 2.62 (d, $^3J_{H,N}$ = 2.9 Hz, 6H), 2.49 (s, 3H) ppm.

S2.3 *Synthesis of [4,4'-Bis(1,1-dimethylethyl)-2,2'-bipyridine-N1,N1']bis[2-(2-pyridinyl-N)phenyl-C]iridium(III) Tetrakis(3,5-bis(trifluoromethyl)phenyl)borate* (**[Ir]**BAr^F_4). $Ir(ppy)_2(dtbbpy)[PF_6]$ (100 mg, 0.11 mmol) and $Na[BAr^F_4]$ (92.2 mg, 0.10 mmol, 0.95 eq) were stirred in 5 mL Et_2O at room temperature for 1 hour. The solution was filtered through celite, layered with pentane and stored at -40°C overnight to yield the title compound as yellow crystals (161 mg, 90% yield). ^{1}H NMR (400 MHz, MeCN-d_3) δ 8.48 (s, 2H), 8.06 (d, 2H, J = 8.2 Hz), 7.93-7.76 (m, 6H), 7.74-7.64 (m, 10H), 7.58 (d, J = 5.8 Hz, 2H), 7.50 (dd, J = 5.9, 1.9 Hz, 2H), 7.03 (t, J = 6.8 Hz, 2H), 6.91 (t, J = 6.8 Hz, 2H), 6.28 (d, J = 6.3 Hz, 2H), 1.40 (s, 18H) ppm.

S3 Ammonia production and quantification studies

S3.1 Standard NH_3 Generation Reaction Procedure

All solvents are stirred with Na/K for ≥2 hours and filtered prior to use. In a nitrogen-filled glovebox, the precatalysts ([Mo]Br_3 and/or [Ir]BAr^F_4) (2.3 μmol) are weighed in individual vials.* The precatalysts are then transferred quantitatively into a Schlenk tube using THF. The THF is then evaporated to provide a thin film of precatalyst at the bottom of the Schlenk tube. The tube is then charged with a stir bar and the acid and Hantzsch ester (HEH_2) are added as solids. The tube is cooled to 77 K in a cold well. The base ([Col]) is dissolved in 1 mL solvent. To the cold tube is added the 1 mL solution of base and solvent to produce a concentration of precatalyst of 2.3 mM. The temperature of the system is allowed to equilibrate for 5 minutes and then the tube is sealed with a Teflon screw-valve. This tube is passed out of the box into a liquid N_2 bath and transported to a fume hood. For experiments run at -78 ℃ the tube is then transferred to a dry ice/isopropanol bath where it thaws and is allowed to stir under blue LED irradiation at -78 °C for minimum three hours before warming. For experiments run at 23 ℃ the tube is instead transferred to a water bath where it thaws and is allowed to stir for 12 hours. To ensure reproducibility, all experiments were conducted in 200 mL Schlenk tubes (50 mm OD) using 10 mm eggshaped-stir bars and stirring was conducted at ~600 rpm. Both the water bath and the dry ice/isopropanol bath were contained in highly reflective dewars. The Blue LED was placed above the bath as close to the stirring reaction as possible.

* In cases where less than 2.3 μmol of precatalyst were used, stock solutions were used to avoid having to weigh very small amounts.

S3.2 NH_3 Generation Reaction Procedure under Partial H_2 Atmosphere

Catalytic runs done under a mixture of H_2 and N_2 were conducted similarly to those under N_2 atmosphere, with a few differences described below. The loadings were the same as in Table 1, Entry 9.

Catalysis is performed in the same Schlenk tubes as under N_2, which are charged with precatalyst, HEH_2, [ColH]OTf, and a stirbar in a nitrogen-filled glovebox as described above. After addition of the solids, the tube is wrapped in aluminum foil and the base (Col) is added in 1 mL of Na/K dried THF at room temperature. Half of the headspace volume is then removed using a calibrated bulb and then backfilled with H_2 which has been passed through a liquid nitrogen trap. The aluminum foil is removed and the reaction is allowed to stir under Blue LED irradiation for 12 hours. Variation from the standard procedure (addition of THF/Col at room temperature and allowing to stir without irradiation for 30 min before exposing to blue LED) were found to not perturb the yield of NH_3.

Figure S1. Set-up for catalysis with Schlenk tube, stir plate, Kessil® 34 W 150 Blue lamp and dewar. Lamp is turned off for clarity.

S3.3 NH_3 detection by optical methods

Reaction mixtures are cooled to 77 K and allowed to freeze. The reaction vessel is then opened to atmosphere and to the frozen solution is slowly added excess of a solution of HCl (3 mL of a 2.0 M solution in Et_2O, 6 mmol) over 1-2 minutes. This solution is allowed to freeze, then the headspace of the tube is evacuated and the tube is sealed. The tube is then allowed to warm to RT and stirred at RT for at least 10 minutes. Solvent is removed *in vacuo*, and the solids are extracted with 1 M HCl(aq) and filtered to give a total solution volume of 10 mL. A 5 mL aliquot is taken and washed repeatedly with n-butanol to remove Hantzsch pyridine (HE) and collidinium. After n-butanol washing additional 1 M HCl(aq) is added to give a final total volume of 5 mL. From these 5 mL solutions, a 100 µL aliquot is analyzed for the presence of NH_3 (present as $[NH_4][Cl]$) by the indophenol method. Quantification was performed with UV-vis spectroscopy by analyzing the absorbance at 635 nm.[9] When specified a further aliquot of this solution was analyzed for the presence of N_2H_4 (present as $[N_2H_5][Cl]$) by a standard colorimetric method.[10] Quantification was performed with UV-vis spectroscopy by analyzing the absorbance at 458 nm.

S3.4 NH_3 detection by ^1H NMR

Reaction mixtures are cooled to 77 K and allowed to freeze. The reaction vessel is then opened to atmosphere and to the frozen solution is slowly added an excess (with respect to acid) solution of a

NaO^tBu solution in MeOH (0.25 mM) over 1-2 minutes. This solution is allowed to freeze, then the headspace of the tube is evacuated and the tube is sealed. The tube is then allowed to warm to RT and stirred at RT for at least 10 minutes. An additional Schlenk tube is charged with HCl (3 mL of a 2.0 M solution in Et_2O, 6 mmol) to serve as a collection flask. The volatiles of the reaction mixture are vacuum transferred at RT into this collection flask. After completion of the vacuum transfer, the collection flask is sealed and warmed to RT. Solvent is removed in vacuo, and the remaining residue is dissolved in 0.7 mL of DMSO-d_6 containing 20 mM 1,3,5-trimethoxybenzene as an internal standard. Integration of the ^1H NMR peak observed for NH_4^+ is then integrated against the two peaks of trimethoxybenzene to quantify the ammonium present. This ^1H NMR detection method was also used to differentiate [$^{14}NH_4$][Cl] and [$^{15}NH_4$][Cl] produced in the control reactions conducted with $^{15}N_2$, ^{15}N-Col/[ColH]OTf, or ^{15}N-HEH_2.

S3.5 NH_3 detection results

S3.5.1 Catalytic results in main text (Table 1)

Table S1: Catalytic yields for photodriven transfer hydrogenation of N_2 to NH_3.

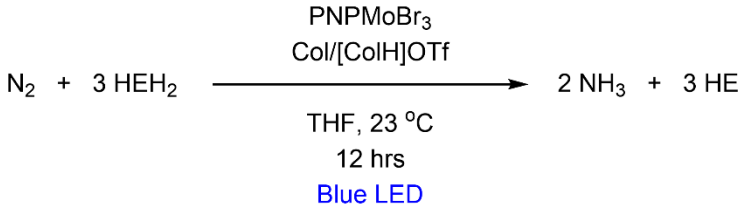

Run	Conditions	[Mo] load (µmol)	acid (µmol)	base (µmol)	Ir (µmol)	HEH_2 equiv /Mo	NH_3 equiv /Mo	N_2H_4 equiv/ Mo	NH_3 yield/ HEH_2 (%)
Table 1, entry 1: Standard conditions									
A1	THF, 23 °C	2.3	124.2	124.2	0	54	9.5	-	
B1	THF, 23 °C	2.3	124.2	124.2	0	54	8.3	-	
C1	THF, 23 °C	2.3	124.2	124.2	0	54	10.8	-	
	THF, 23 °C	2.3	124.2	124.2	0	54	9.5±1		26.5±3
Table 1, entry 2: 0.575 mM [Mo]Br_3									
D1	THF, 23 °C	0.575	124.2	124.2	0	216	22.6	-	
E1	THF, 23 °C	0.575	124.2	124.2	0	216	20.9	-	
	THF, 23 °C	0.575	124.2	124.2	0	216	21.8±0.8		15.1±06
Table 1, entry 3: No light									
F1	THF, 23 °C no light	2.3	124.2	124.2	0	54	<0.1	<0.1	
G1	THF, 23 °C no light	2.3	124.2	124.2	0	54	<0.1	<0.1	
	THF, 23 °C no light	2.3	124.2	124.2	0	54	<0.1	<0.1	<0.3
Table 1, entry 4: No buffer									
H1	THF, 23 °C	2.3	**0**	**0**	0	54	0.74	-	
I1	THF, 23 °C	2.3	**0**	**0**	0	54	1.11	-	
	THF, 23 °C	2.3	**0**	**0**	0	54	0.9±0.2		2.6±0.5
Table 1, entry 5: 5 equiv Col/[ColH]OTf									
J1	THF, 23 °C	2.3	11.5	11.5	0	54	2.7	<0.1	
K1	THF, 23 °C	2.3	11.5	11.5	0	54	3.2	<0.1	
L1	THF, 23 °C	2.3	11.5	11.5	0	54	2.8	-	
	THF, 23 °C	2.3	11.5	11.5	0	54	2.9±0.2	<0.1	8.1±0.6
Table 1, entry 6: benzene instead of THF									
M1	C_6H_6, 23 °C	2.3	124.2	124.2	0	54	4.8	-	
N1	C_6H_6, 23 °C	2.3	124.2	124.2	0	54	4.6	-	
	C_6H_6, 23 °C	2.3	124.2	124.2	0	54	4.7±0.1		13±0.3

Run	Conditions	[Mo] load (μmol)	acid (μmol)	base (μmol)	Ir (μmol)	HEH_2 equiv /Mo	NH_3 equiv /Mo	N_2H_4 equiv /Mo	NH_3 yield/ HEH_2 (%)
Table 1, entry 7: 216 equiv Col/[ColH]OTf									
O1	THF, 23 ℃	2.3	496.8	496.8	0	54	19.5	-	
P1	THF, 23 ℃	2.3	496.8	496.8	0	54	21.1	-	
	THF, 23 ℃	2.3	496.8	496.8	0	54	20.3±0.8		56±2
Table 1, entry 8: with 10 equiv TBABr									
Q1	THF, 23 ℃	2.3	124.2	124.2	0	54	9	-	
R1	THF, 23 ℃	2.3	124.2	124.2	0	54	8.6	-	
	THF, 23 ℃	2.3	124.2	124.2	0	54	8.8±0.3		23.6±0.8
Table 1, entry 9: Added [Ir]BAr^F_4									
S1	THF, 23 ℃	2.3	124.2	124.2	2.3	54	29.8	-	
T1	THF, 23 ℃	2.3	124.2	124.2	2.3	54	20.6	-	
U1	THF, 23 ℃	2.3	124.2	124.2	2.3	54	20.5	-	
V1	THF, 23 ℃	2.3	124.2	124.2	2.3	54	25.4	-	
	THF, 23 ℃	2.3	124.2	124.2	2.3	54	24±4		67±10
Table 1, entry 10: Added [Ir]BAr^F_4, 5 equiv Col/[ColH]OTf									
W1	THF, 23 ℃	2.3	11.5	11.5	2.3	54	16.02	<0.1	
X1	THF, 23 ℃	2.3	11.5	11.5	2.3	54	16.6	<0.1	
Y1	THF, 23 ℃	2.3	11.5	11.5	2.3	54	14.7		
	THF, 23 ℃	2.3	11.5	11.5	2.3	54	15.8±0.8	<0.1	44±2
Table 1, entry 11: Added [Ir]BAr^F_4, t = ½ h									
Z1	THF, 23 ℃ t = ½ h	2.3	124.2	124.2	2.3	54	19.5	-	
AA1	THF, 23 ℃ t = ½ h	2.3	124.2	124.2	2.3	54	17.7	-	
	THF, 23 ℃ t = 1/2 h	2.3	124.2	124.2	2.3	54	18.6±0.9		52±3
~75 % completion compared to entry 8									
Table 1, entry 12: t = 2 h									
AB1	THF, 23 ℃ t = 2 h	2.3	124.2	124.2	0	54	4.9	-	
AC1	THF, 23 ℃ t = 2 h	2.3	124.2	124.2	0	54	7.9	-	
AD1	THF, 23 ℃ t = 2 h	2.3	124.2	124.2	0	54	10	-	
	THF, 23 ℃ t = 2 h	2.3	124.2	124.2	0	54	7.6±2		21±6
~80 % completion compared to entry 1									
Table 1, entry 13: Added [Ir]BAr^F_4, 5 equiv Col/[ColH]OTf, 0.575 mM $[Mo]Br_3$									
AE1	THF, 23 ℃	0.575	11.5	11.5	2.3	216	26.83	-	
AF1	THF, 23 ℃	0.575	11.5	11.5	2.3	216	25.96	-	
	THF, 23 ℃	0.575	11.5	11.5	2.3	216	26±0.4		18.4±0.4
Table 1, entry 14: Added [Ir]BAr^F_4, 5 equiv Col/[ColH]OTf, no light									
AG1	THF, 23 ℃ no light	2.3	11.5	11.5	2.3	54	<0.1	<0.1	
AH1	THF, 23 ℃ no light	2.3	11.5	11.5	2.3	54	<0.1	<0.1	
	THF, 23 ℃ no light	2.3	11.5	11.5	2.3	54	<0.1	<0.1	<0.3

Run	Conditions	[Mo] load (μmol)	acid (μmol)	base (μmol)	Ir (μmol)	HEH_2 equiv /Mo	NH_3 equiv /Mo	N_2H_4 equiv/ Mo	NH_3 yield/ HEH_2 (%)
Table 1, entry 15: Added [Ir]BAr^F_4, 5 equiv Col/[ColH]OTf, no [Mo]Br_3									
AI1	THF, 23 °C	**0**	11.5	11.5	2.3	54	<0.1	<0.1	
AJ1	THF, 23 °C	**0**	11.5	11.5	2.3	54	<0.1	<0.1	
	THF, 23 °C	**0**	11.5	11.5	2.3	54	<0.1	<0.1	<0.3
Table 1, entry 16: Added [Ir]BAr^F_4, 5 equiv Col/[ColH]OTf, no HEH_2									
AK1	THF, 23 °C	2.3	11.5	11.5	2.3	**0**	<0.1	<0.1	
AL1	THF, 23 °C	2.3	11.5	11.5	2.3	**0**	<0.1	<0.1	
	THF, 23 °C	2.3	11.5	11.5	2.3	**0**	<0.1	<0.1	<0.3
Table 1, entry 17: Added [Ir]BAr^F_4, subH_2 = 9,10-dihydroacridine									
AM1	THF, 23 °C	2.3	124.2	124.2	2.3	54[a]	6.7	-	
AN1	THF, 23 °C	2.3	124.2	124.2	2.3	54[a]	6.1	-	
	THF, 23 °C	2.3	124.2	124.2	2.3	54[a]	6.4±0.3		17.7±0.8
[a]9,10-dihydroacridine used instead of HEH_2									
Table 1, entry 18: Added [Ir]BAr^F_4, subH_2 = 5,6-dihydrophenanthridine									
AO1	THF, 23 °C	2.3	124.2	124.2	2.3	54[b]	4.5	-	
AP1	THF, 23 °C	2.3	124.2	124.2	2.3	54[b]	5.1	-	
	THF, 23 °C	2.3	124.2	124.2	2.3	54[b]	4.6±0.8		13±2
[b]5,6-dihydrophenanthridine used instead of HEH_2									
Table 1, entry 19: Added [Ir]BAr^F_4, subH_2 = 1-benzyl-1,4-dihydronicotinamide									
AQ1	THF, 23 °C	2.3	124.2	124.2	2.3	54[c]	1.31	-	
AR1	THF, 23 °C	2.3	124.2	124.2	2.3	54[c]	1.12	-	
	THF, 23 °C	2.3	124.2	124.2	2.3	54[c]	1.2±0.1		3.3±0.3
[c]1-benzyl-1,4-dihydronicotinamide used instead of HEH_2									
Table 1, entry 20: Added [Ir]BAr^F_4, 0.5 atm H_2, 0.5 atm N_2									
AS1	THF, 23 °C $P_{N2} = P_{H2}$ = 0.5 atm	2.3	124.2	124.2	2.3	54	16.1	-	
AT1	THF, 23 °C $P_{N2} = P_{H2}$ = 0.5 atm	2.3	124.2	124.2	2.3	54	11.0	-	
	THF, 23 °C $P_{N2} = P_{H2}$ = 0.5 atm	2.3	124.2	124.2	2.3	54	14±4		36±9
Table 1, entry 21: Added [Ir]BAr^F_4, no Col/[ColH]OTf									
AU1	THF, 23 °C	2.3	**0**	**0**	2.3	54	7.03	-	
AV1	THF, 23 °C	2.3	**0**	**0**	2.3	54	7.83	-	
	THF, 23 °C	2.3	**0**	**0**	2.3	54	7.4±0.4		20.7±1

S3.5.2 Additional catalytic experiments

Table S2 Canvassing H_2 carriers

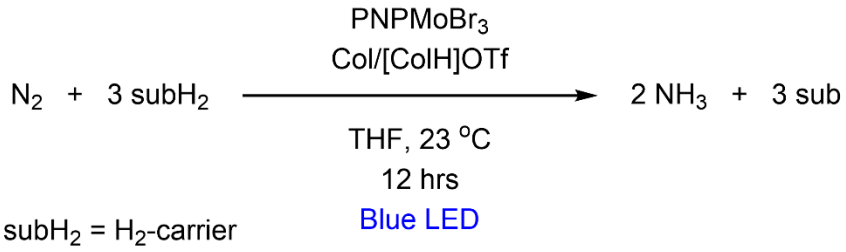

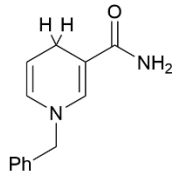

BNAH
(1-benzyl-1,4-dihydronicotinamide)

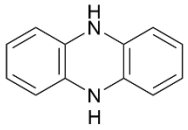

phenazH$_2$
(5,10-dihydrophenazine)

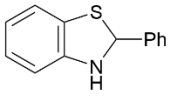

BTH$_2$
(2-phenylbenzothiazolin)

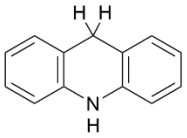

acrH$_2$
(9,10-dihydroacridine)

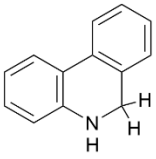

phenH$_2$
(5,6-dihydrophenanthridine)

Run	subH$_2$	[Mo]Br$_3$ load (µmol)	acid (µmol)	base (µmol)	Ir (µmol)	subH$_2$ equiv /Mo	NH$_3$ equiv /Mo	N$_2$H$_4$ equiv/Mo	NH$_3$ yield/ subH$_2$ (%)
A2	BNAH	2.3	124.2	124.2	**0**	54	0.55	-	
B2	BNAH	2.3	124.2	124.2	**0**	54	0.30	-	
	BNAH	2.3	124.2	124.2	**0**	54	0.4±0.1		1.2±0.3
C2	PhenazH$_2$	2.3	124.2	124.2	**2.3**	54	<0.1	-	
D2	PhenazH$_2$	2.3	124.2	124.2	**2.3**	54	<0.1	-	
	PhenazH$_2$	2.3	124.2	124.2	**2.3**	54	<0.1		<0.1
E2	BTH$_2$	2.3	124.2	124.2	**2.3**	54	<0.1	-	
F2	BTH$_2$	2.3	124.2	124.2	**2.3**	54	<0.1	-	
	BTH$_2$	2.3	124.2	124.2	**2.3**	54	<0.1		<0.1
G2	AcrH$_2$	2.3	124.2	124.2	**0**	54	0.09	-	
H2	AcrH$_2$	2.3	124.2	124.2	**0**	54	0.24	-	
	AcrH$_2$	2.3	124.2	124.2	**0**	54	0.16±0.08		0.5±0.2
I2	PhenH$_2$	2.3	124.2	124.2	**0**	54	0.216	-	
J2	PhenH$_2$	2.3	124.2	124.2	**0**	54	0.205	-	
	PhenH$_2$	2.3	124.2	124.2	**0**	54	0.211±0.008		0.66±0.02

Table S3. Additional time course experiments

Run	Conditions	Mo loading (µmol)	acid (µmol)	base (µmol)	Ir (µmol)	HEH_2 equiv /Mo	NH_3 equiv /Mo	N_2H_4 equiv/Mo	NH_3 yield/ HEH_2 (%)
A3	THF, 23 °C t = 2 h	2.3	124.2	124.2	2.3	54	24.5	-	
B3	THF, 23 °C t = 2 h	2.3	124.2	124.2	2.3	54	25.5	-	
	THF, 23 °C t = 2 hours	2.3	124.2	124.2	2.3	54	25±0.5		69.4±1.5
Approximately 100% completion compared to Table 1, entry 8									
C3	THF, rt, 10 min	2.3	124.2	124.2	2.3	54	8.2	-	22.8
Approximately 30% completion compared to Table 1, entry 8									

Table S4 Catalysis using [ColH]OTf or Col instead of buffered solution

Run	Conditions	Mo loading (µmol)	acid (µmol)	base (µmol)	Ir (µmol)	HEH_2 equiv /Mo	NH_3 equiv /Mo	N_2H_4 equiv/Mo	NH_3 yield/ HEH_2 (%)
A4	THF, 23°C	2.3	496.8	**0**	**0**	54	5.8	-	
B4	THF, 23°C	2.3	496.8	**0**	**0**	54	5.5	-	
	THF, 23°C	2.3	496.8	**0**	**0**	54	5.65±.15		15.7±0.4
C4	THF, 23°C	2.3	**0**	496.8	**0**	54	1.2	-	
D4	THF, 23°C	2.3	**0**	496.8	**0**	54	2.0	-	
	THF, 23°C	2.3	**0**	496.8	**0**	54	1.6±0.4		4.7±1.1

Table S5. Optimization of [Ir]BAr$^F_4$, 5 equiv Col/[ColH]OTf conditions

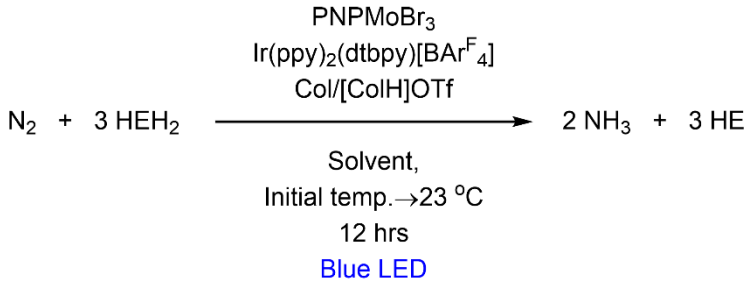

Run	Conditions	Mo loading (µmol)	acid (µmol)	base (µmol)	Ir (µmol)	HEH_2 equiv /Mo	NH_3 equiv /Mo	N_2H_4 equiv/Mo	NH_3 yield/ HEH_2 (%)
A5	THF, -78 →23°C	2.3	11.5	11.5	2.3	54	15.47	-	
B5	THF, -78 →23°C	2.3	11.5	11.5	2.3	54	16.06	-	
	THF, -78 →23°C	2.3	11.5	11.5	2.3	54	15.7±0.3		44.8±0.8
C5	Tol, 23°C	2.3	11.5	11.5	2.3	54	7	-	
D5	Tol, 23°C	2.3	11.5	11.5	2.3	54	7.3	-	
	Tol 23°C	2.3	11.5	11.5	2.3	54	7.15±0.15		19.8±0.8
E5	Tol, -78 →23°C	2.3	11.5	11.5	2.3	54	13.01	-	
F5	Tol, -78 →23°C	2.3	11.5	11.5	2.3	54	14.24	-	
	Tol, -78 →23°C	2.3	11.5	11.5	2.3	54	13.6±0.6		38±2
G5	Et_2O, -78 →23°C	2.3	11.5	11.5	2.3	54	4.08	-	
H5	Et_2O, -78 → 23°C	2.3	11.5	11.5	2.3	54	3.97	-	
	Et_2O, -78 → 23°C	2.3	11.5	11.5	2.3	54	4.0±0.1		11.2±0.2
I5	THF, -78 →23°C	2.3	11.5	11.5	2.3[a]	54	7.4	-	
J5	THF, -78 →23°C	2.3	11.5	11.5	2.3[a]	54	11.7	-	
	THF, -78 →23°C	2.3	11.5	11.5	2.3[a]	54	9.6±2		27±7

[a]$Ir(ppy)_3$ used as photosensitizer
Tol = toluene

S3.6 NH_3 detection results from ^{15}N-HEH_2, ^{15}N-Col/^{15}N-[ColH]OTf and $^{15}N_2$ experiments

S3.6.1 $^{15}N_2$ experiments

Catalytic runs done under a $^{15}N_2$ atmosphere were conducted similarly to those under a $^{14}N_2$ atmosphere, with a few differences described below. The loadings were the same as in Table 1, Entry 1.

Catalysis is performed in the same catalytic tubes as natural abundance experiments, which are charged with precatalyst, HEH_2, [ColH]OTf, and a stirbar in a nitrogen-filled glovebox as described above. After addition of the solids, the tube is then cooled to 77 K in a cold well. The base (Col) is added by micropipette to the frozen tube by opening the Kontes. The Kontes was closed and the tube is kept frozen, then passed out of the glovebox into a liquid N_2 bath. The headspace of the tube is evacuated while still submerged in liquid N_2.

Na/K dried THF is filtered and 1 mL placed into a separate Schlenk tube. The solvent undergoes freeze-pump thaw cycles (3 cycles) and is then vacuum transferred into the catalysis tube. This tube is allowed to warm up briefly and charged with $^{15}N_2$ via vacuum bridge. The tube is refrozen at 77 K and then transferred to a water bath where it thaws and is allowed to stir under Blue LED irradiation for 12 hours.

S3.6.2 ^{15}N-HEH_2, ^{15}N-Col/^{15}N-[ColH]OTf experiments

Catalytic runs were set-up as described in **S3.1** but using either ^{15}N-HEH_2 as H_2-carrier or ^{15}N-Col/[ColH]OTf as buffer using the same conditions as Table 1, Entry 1.

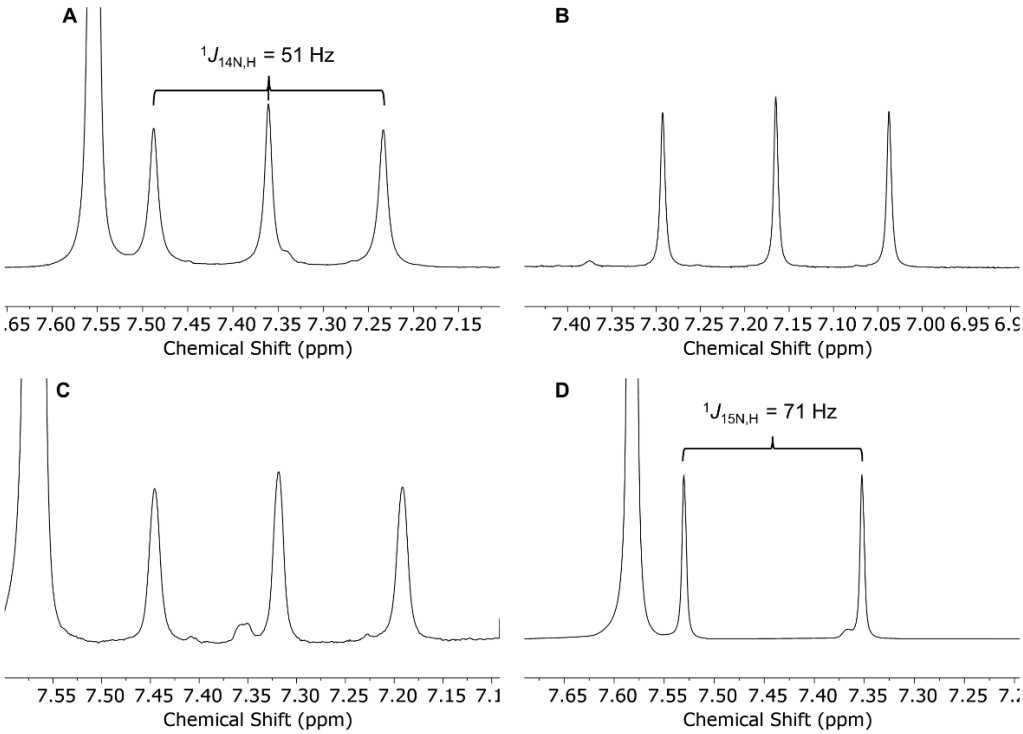

Figure S2. ^{1}H NMR (DMSO-d_6, 400 MHz) of: A) $^{14}NH_4Cl$ obtained from reaction of natural abundance reactants under $^{14}N_2$ (Ir-free conditions in Table 1, entry 1); B) $^{14}NH_4Cl$ obtained from reaction of ^{15}N-labeled HEH_2 (otherwise natural abundance reactants) under $^{14}N_2$ (Ir-free conditions in Table 1, entry 1); C) $^{14}NH_4Cl$ obtained from reaction of ^{15}N-labeled Col/[ColH]OTf (otherwise natural abundance reactants) under $^{14}N_2$ (Ir-free conditions in Table 1, entry 1); D) $^{15}NH_4Cl$ obtained from reaction under $^{15}N_2$ (otherwise natural abundance reactants, Ir-free conditions in Table 1, entry 1).

S4.1 Analysis of non-NH_3 catalysis products:

After a complete catalytic run, instead of quenching the reaction (with acid or base) the solvent from the reaction mixture was removed *in vacuo*. Subsequently the resulting film was taken up in minimal solvent (DMSO-d_6, THF-d_8 or 2-MeTHF) and analyzed by NMR or CW-EPR.

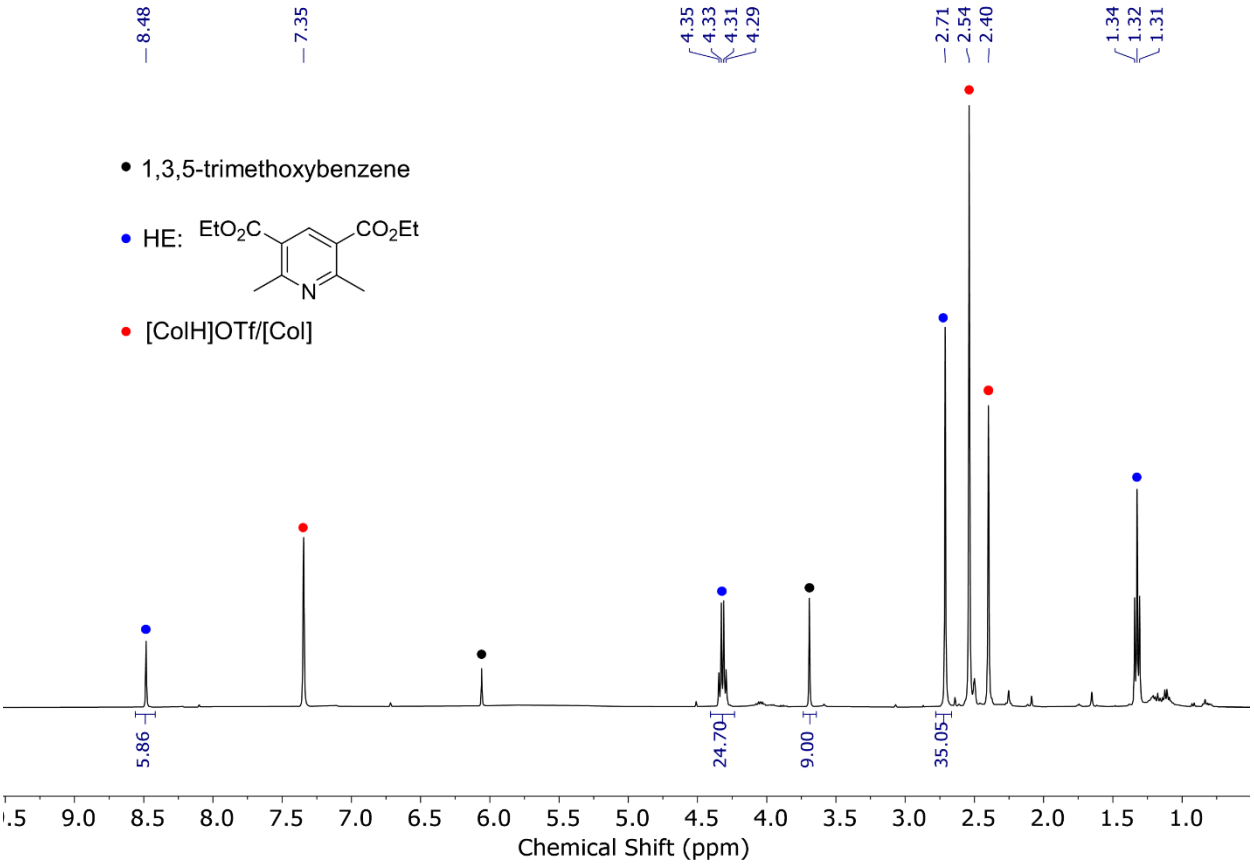

Figure S3. ^{1}H NMR (DMSO-d_6, 400 MHz) of the nonvolatile products of the Mo-catalyzed reaction of HEH_2, [ColH]OTf, [Col], and N_2 under blue LED irradiation (Table 1, entry 1). Integration to 1,3,5-trimethoxybenzene as internal standard (14 µmol) indicates 65% yield of HE as the major product.

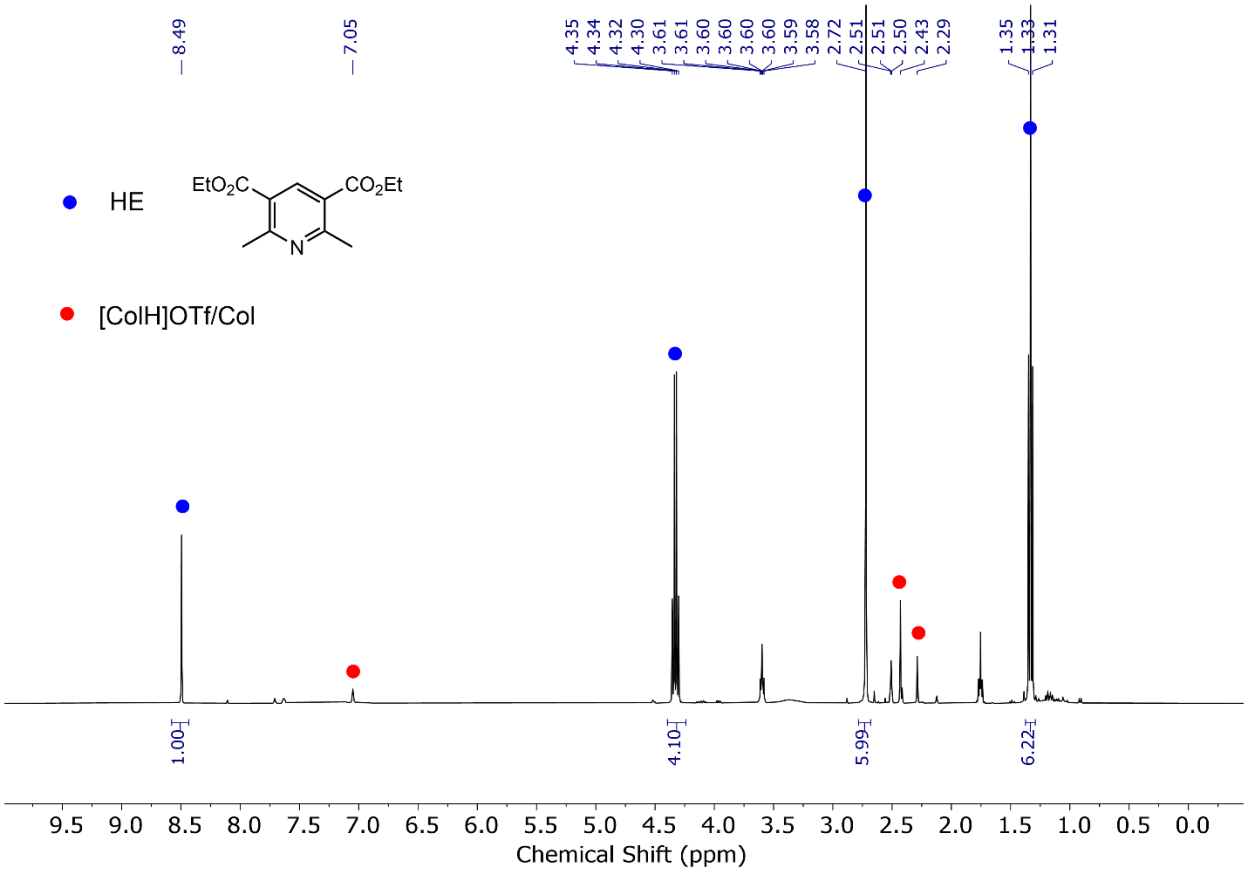

Figure S4. ^{1}H NMR (DMSO-d_6, 400 MHz) of the nonvolatile products of the Col/[ColH]OTf-, Ir- and Mo-catalyzed reaction of HEH_2 and N_2 under blue LED irradiation (Table 1, entry 9).

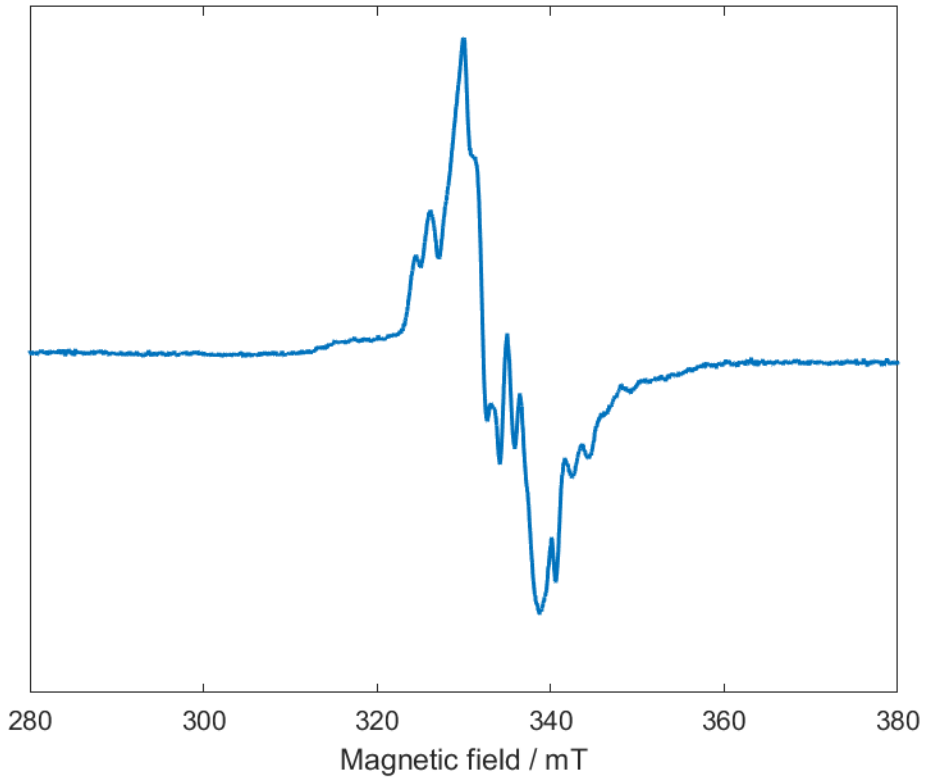

Figure S5. CW-EPR spectrum (2-MeTHF, 77 K) of non-volatile products post-catalysis (conditions in table 1, entry 1). Mixture of unknown [Mo] products are observed.

S4.2 ^{1}H NMR time course experiments

Procedure: A J.Young NMR tube was loaded with [Mo]Br_3, HEH_2, [ColH]OTf, Col, and N_2 and irradiated under blue LED. Conditions (concentration, temperature) were the same as in Table 1, entry 1, but using THF-d_8 as solvent and 0.5 mL solvent instead of 1 mL). Slightly slower reaction times are attributed to less efficient illumination of and lack of stirring in the NMR tube compared to Schlenk flasks.

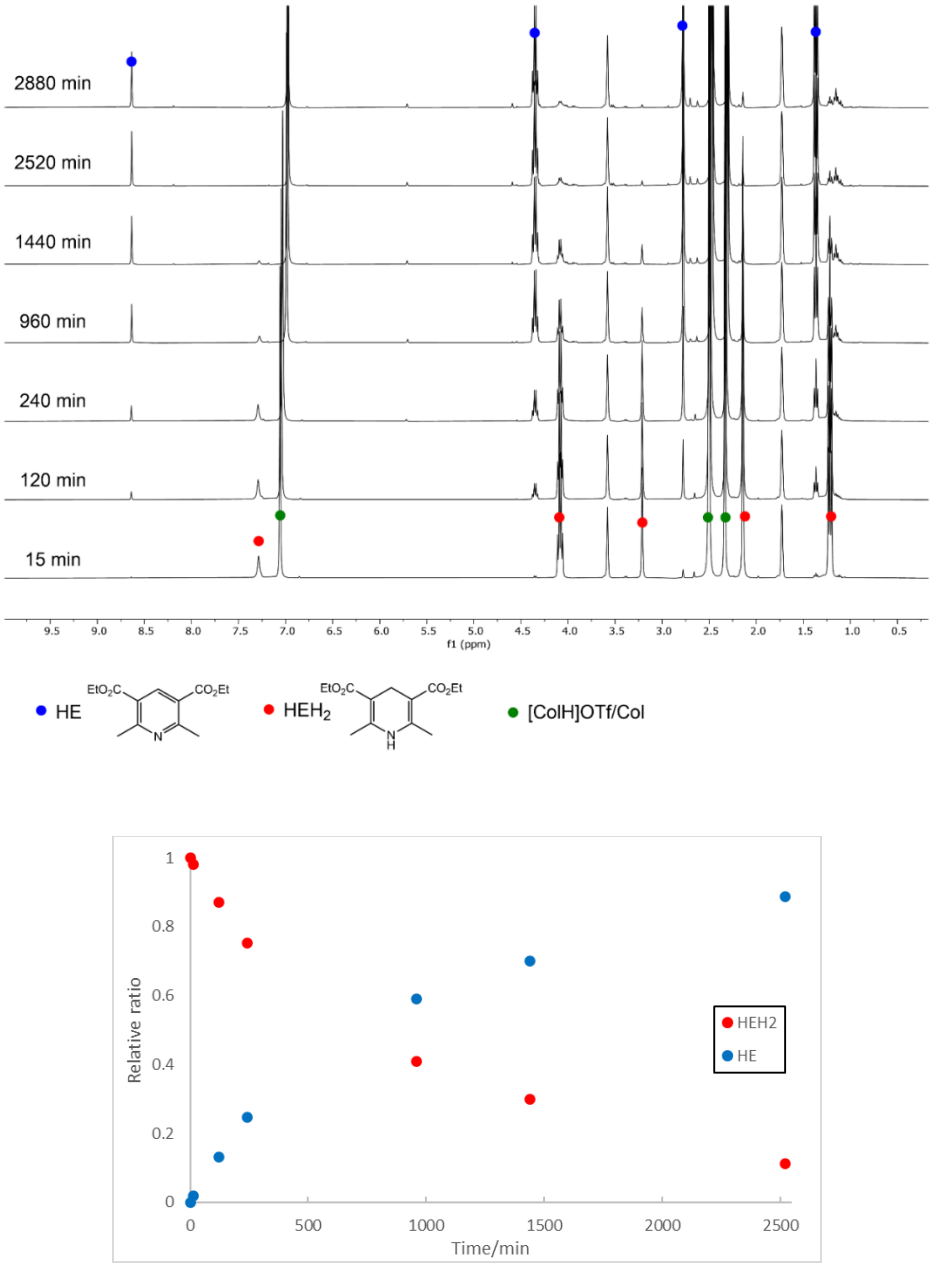

Figure S6. ^{1}H NMR (THF-d_8, 400 MHz) time course of the Mo-catalyzed reaction of HEH_2, [ColH]OTf, Col, and N_2 under blue LED irradiation in a J. Young tube (Table 1, entry 1) (Top). Relative ratio of HE and HEH_2 plotted over time (bottom).

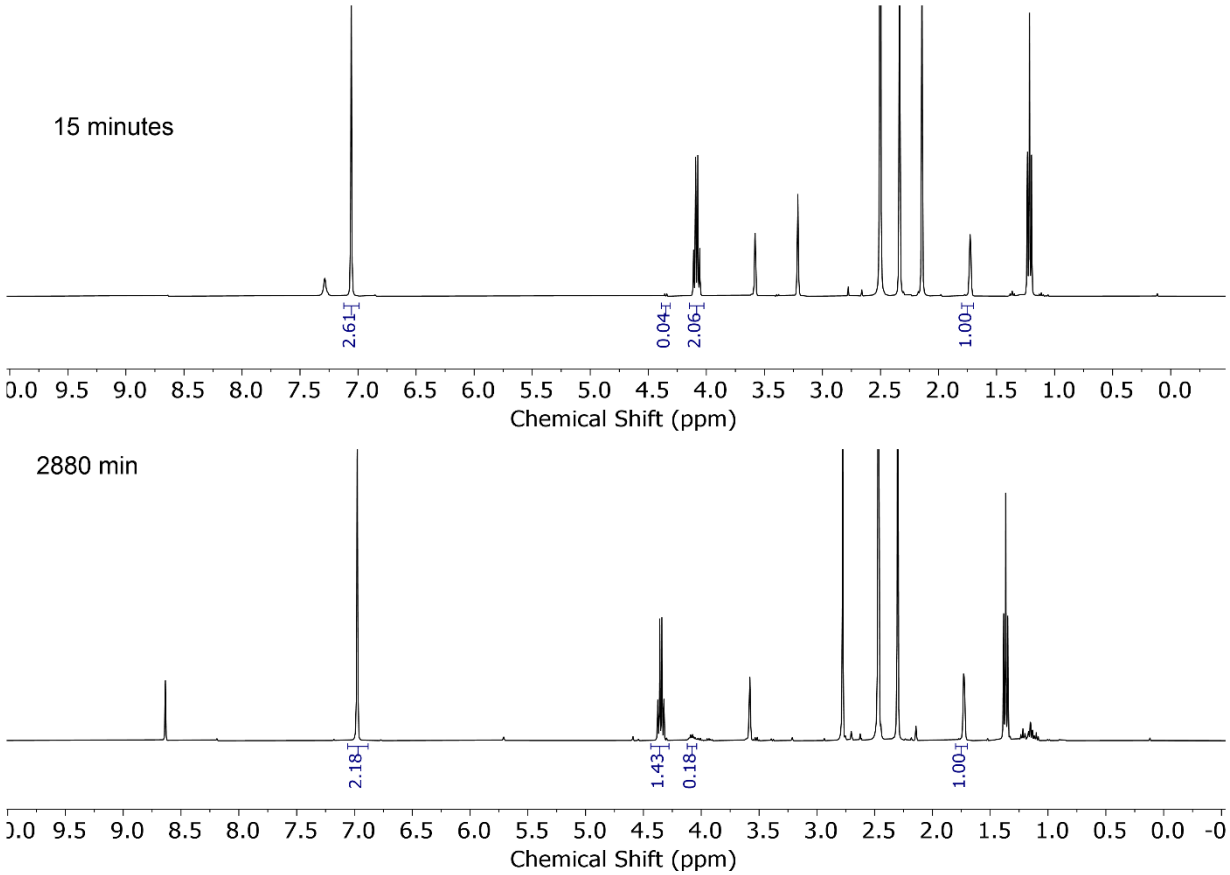

Figure S7. ^{1}H NMR (THF-d_8, 400 MHz) of 15 minutes and 48 hour time points of the reaction of the Mo-catalyzed reaction of HEH_2, [ColH]OTf, Col, and N_2 under blue LED irradiation in a J.Young tube (Figure S5). Integrals of HEH_2 and HE quartet peak at ~ 4.0 ppm are compared to constant THF solvent residual peaks to estimate total recovery of HEH_2 and HE. Approx. 80% is recovered. Similarly, integrals of Col/[ColH]OTf aromatic peak at ~ 7.0 ppm are compared to constant THF solvent residual peaks to estimate total recovery ofCol/[ColH]OTf. Approx. 80% is recovered.

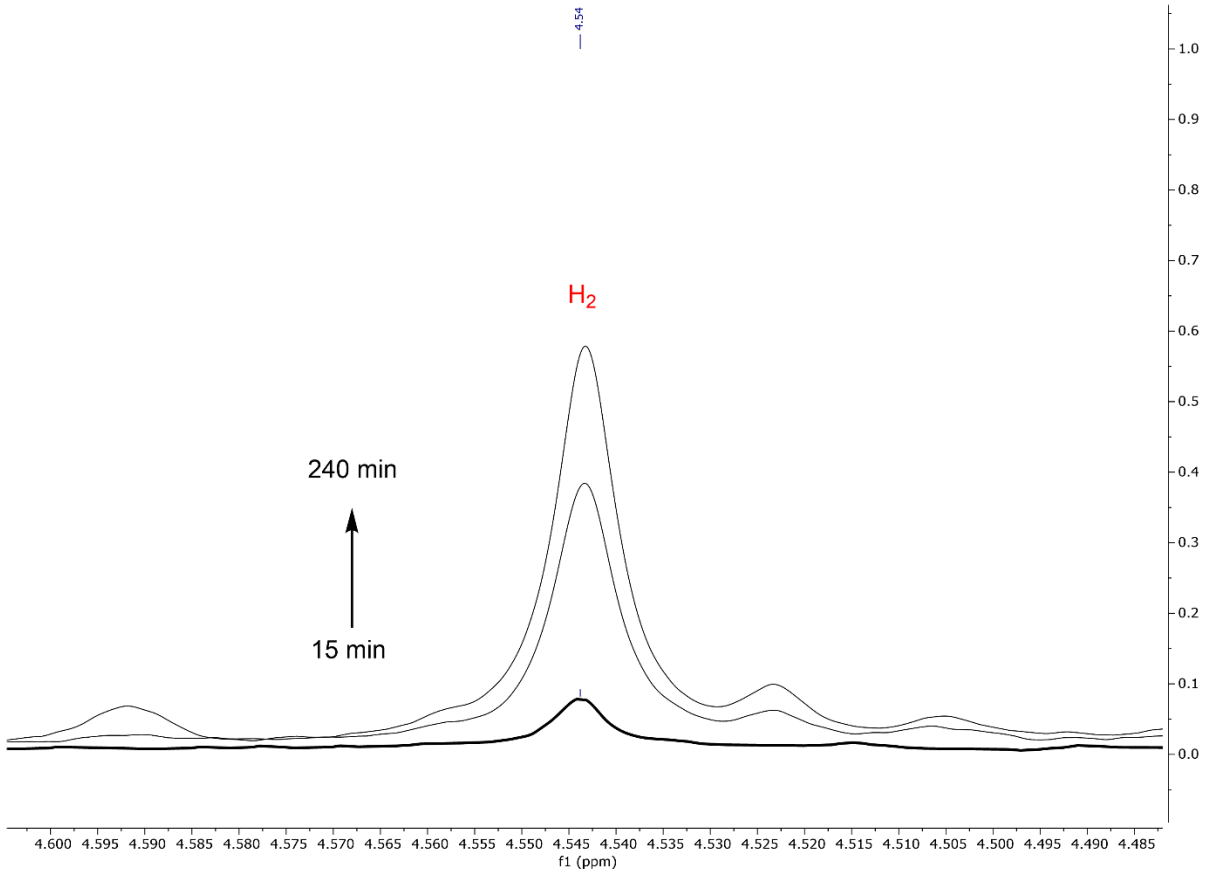

Figure S8. ^{1}H NMR (THF-d_8, 400 MHz) of 15 minutes to 240 min of the Mo-catalyzed reaction of HEH_2, [ColH]OTf, Col, and N_2 under blue LED irradiation in a J.Young tube (Figure S5). The H_2 peak (4.54 ppm, ref. 8) grows in over time.

S5 Steady-State fluorescence measurements:

Procedure for fluorimetry studies: 1 cm quartz glass cuvettes were loaded with 0.5 mM HEH_2 solutions in dry THF, with varying concentrations of quencher (either Col or [ColH]OTf) in a nitrogen glovebox. Stock solutions were used to assure consistency. Solutions were excited at 390 nm wavelength to avoid interference of the excitation wavelength and steady-state fluorescence spectra. Experiments were conducted at 23 °C.

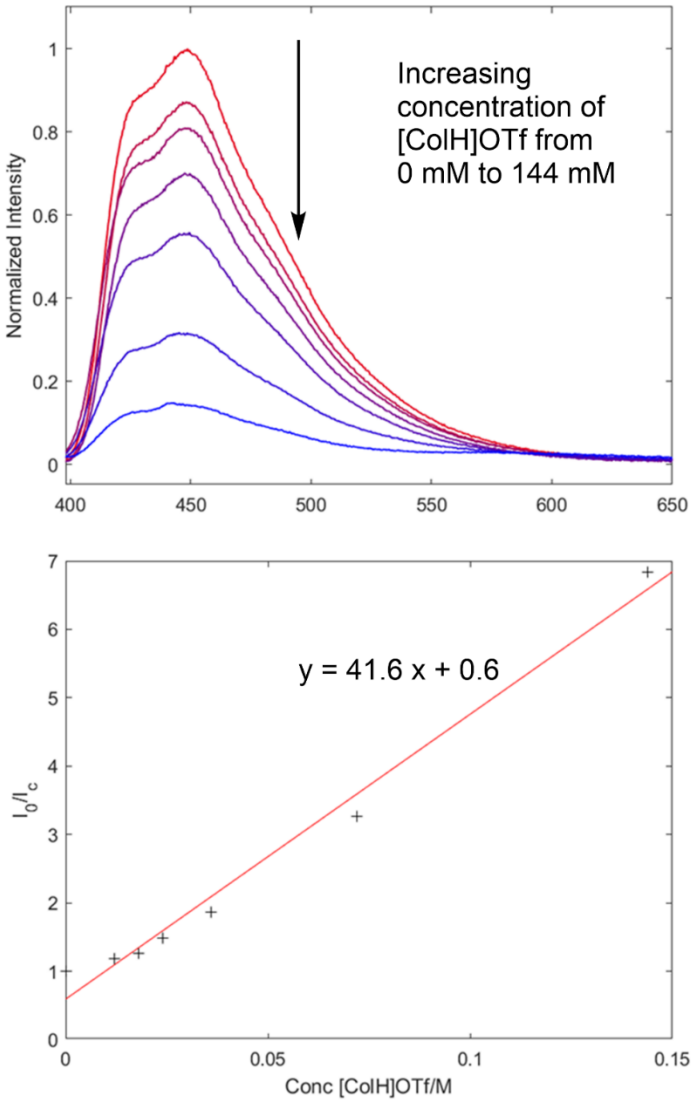

Figure S9. Steady-state fluorescence of HEH_2 (0.5 mM) with varying amounts of [ColH]OTf (18 mM to 144 mM) (Top). Stern-Vollmer quenching plot of I_0/I_C against concentration of [ColH]OTf (bottom).

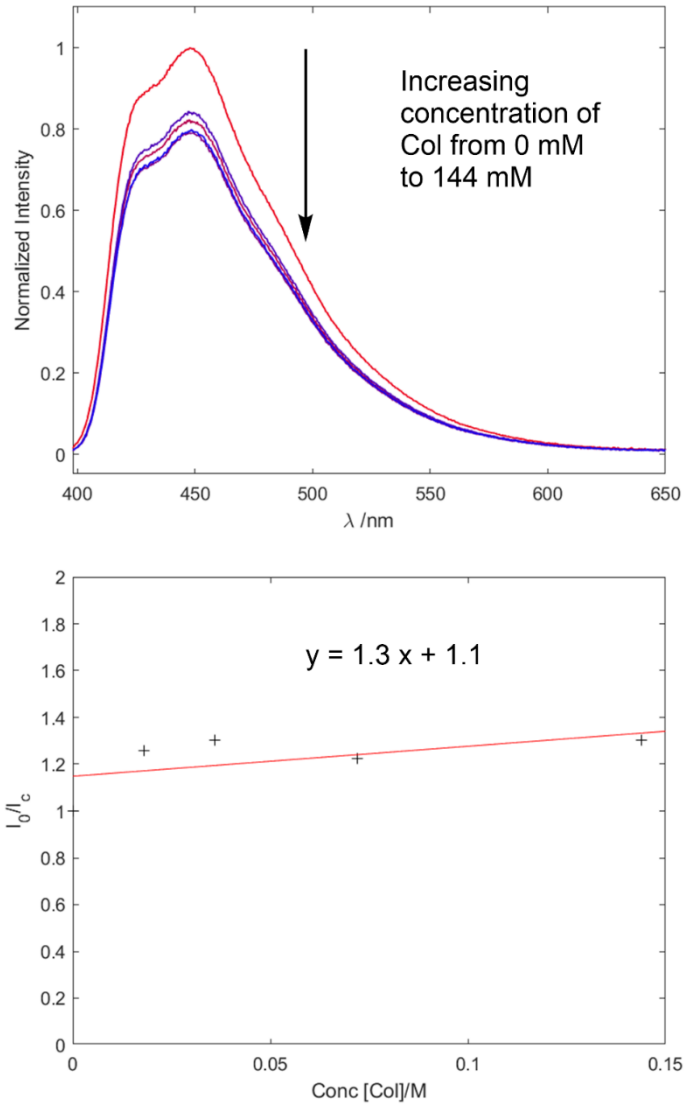

Figure S10. Steady-state fluorescence of HEH_2 (0.5 mM) with varying amounts of Col (18 mM to 144 mM) (Top). Stern-Vollmer quenching plot of I_0/I_C against concentration of Col (bottom).

S6 UV-visible measurements

Procedure for UV-vis measurements: 1 cm quartz glass cuvettes were loaded with 0.1 mM HEH_2 solutions in dry THF inside the glovebox. The cuvette was taken out of the glovebox, and spectra were collected. Concentrated (50 mM) solutions of Col or [ColH]OTf were titrated into the cuvettes. The Col or [ColH]OTf solutions had 0.1 mM HEH_2 added to maintain the HEH_2 concentration throughout the experiments. Titrations were done under a sparging N_2 atmosphere to maintain an O_2 free environment. Experiments were conducted at 23 °C.

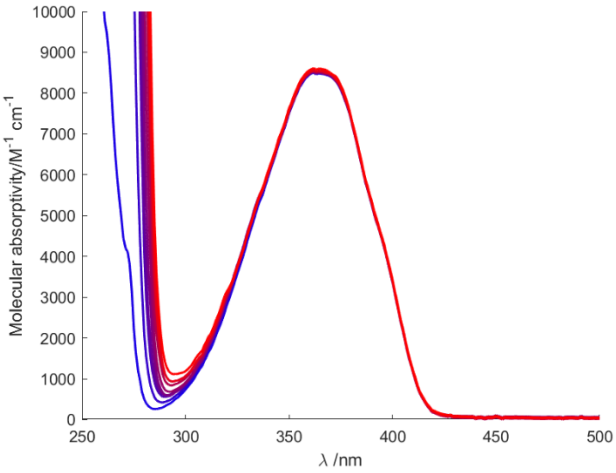

Figure S11. UV-vis of HEH_2 (0.1 mM) with 0 mM (blue) to 14 mM (red) Col concentration.

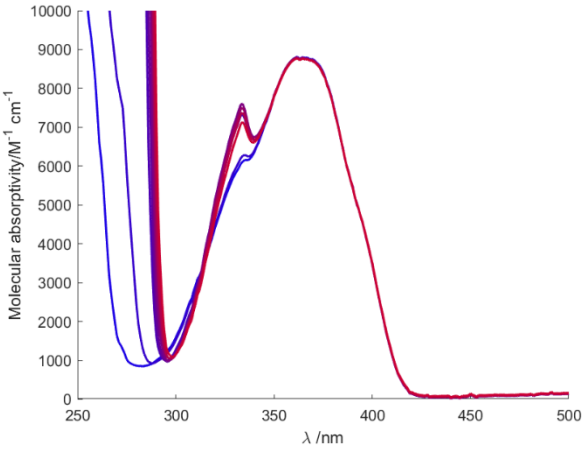

Figure S12. UV-vis of HEH_2 (0.1 mM) with 0 mM (blue) to 11 mM (red) [ColH]OTf concentration.

S7 Derivation of thermodynamic values:

S7.1 Summary of thermochemistry of Hantzsch ester (HEH_2) and derivatives

Table S6 lists $BDFE_{X–H}$, pK_a, and E_{ox} values for various protonation and oxidation states of HEH_2. As has been established by Mayer and coworkers,[11] bond dissociation enthalpies (BDEs) can be converted to BDFEs based on the assumption that the entropies of R–H and R$^\bullet$ are similar. Subtraction of $TS°(H^\bullet)_{solv}$ (6.37 kcal mol^{-1} in MeCN) from the BDE values reported in ref. 3 yields the estimated BDFE values in Table S6. With these values and reported potentials of oxidation, relevant pK_a values were then estimated using the thermodynamic cycles laid out below.

	BDE[a]	**BDFE**[a]	E_{ox}[b]	pK_a
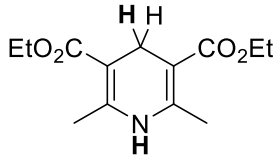 HEH_2	68.7 (C–H), 86.6 (N–H)[c]	62.3 (C–H), 80.2 (N–H)	0.48[c]	31.8 (N–H)
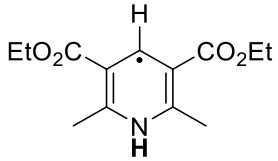 $HEH^\bullet$	46.9 (N–H)[c]	40.5 (N–H)		
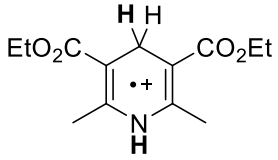 $HEH^{\bullet+}$				–1.0 (C–H)
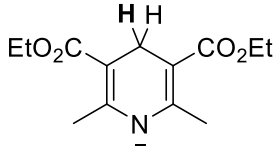 HEH^-			–0.695[c]	
$[HEH_2]$*		–8.5 (C–H)[d]	–2.6[d]	–20(N–H)[d]

Table S6. Reported and estimated thermochemical values for various protonation and oxidation states of HEH_2 relevant to this study. [a] kcal mol^{-1} in MeCN at 298 K. [b] V vs. $Fc^{+/0}$ in MeCN at 298 K. [c] Ref. 3. [d] Estimated using the E_{00} reported in ref. 12.

Estimation of the N–H pK_a of HEH_2:

$HEH^\bullet + e^- \rightleftharpoons HEH^-$	$-23.06(E_{ox}(HEH^-)) = 16$ kcal mol^{-1}
$H^\bullet \rightleftharpoons H^+ + e^-$	$-C_G = -52.6$ kcal mol^{-1}
$HEH_2 \rightleftharpoons HEH^\bullet + H^\bullet$	$BDFE_{N–H}(HEH_2) = 80.2$ kcal mol^{-1}
$HEH_2 \rightleftharpoons HEH^- + H^+$	1.37(pK_a)
	p$K_{a,N–H}(HEH_2)$ = **31.8**

Estimation of the C–H pK_a of $HEH_2^{\bullet+}$:

$HEH_2^{\bullet} + e^- \rightleftharpoons HEH_2$	$-23.06(E_{ox}(HEH_2)) = -11.1$ kcal mol^{-1}
$H^{\bullet} \rightleftharpoons H^+ + e^-$	$-C_G = -52.6$ kcal mol^{-1}
$HEH_2 \rightleftharpoons HEH^{\bullet} + H^{\bullet}$	$BDFE_{C-H}(HEH_2) = 62.3$ kcal mol^{-1}
$HEH_2^{\bullet+} \rightleftharpoons HEH^{\bullet} + H^+$	1.37(pK_a)
	p$K_{a,C-H}(HEH^{\bullet+})$ = **–1.0**

Estimation of the excited-state N–H pK_a of [HEH_2]*:

$HEH_2^* \rightleftharpoons HEH_2$	$-23.06(E_{00}) = -70.8$ kcal mol^{-1}
$HEH_2 \rightleftharpoons HEH^- + H^+$	1.37(p$K_{a,N-H}(HEH_2)$) = 43.6 kcal mol^{-1}
$HEH_2^* \rightleftharpoons HEH^- + H^+$	1.37(pK_a)
	p$K_{a,N-H}(HEH_2^*)$ = **–20**

Estimation of the excited-state $BDFE_{C-H}$ of [HEH_2]*:

$HEH_2^* \rightleftharpoons HEH_2$	$-23.06(E_{00}) = -70.8$ kcal mol^{-1}
$HEH_2 \rightleftharpoons HEH^- + H^+$	$BDFE_{C-H}(HEH_2) = 62.3$ kcal mol^{-1}
$HEH_2^* \rightleftharpoons HEH^- + H^+$	$BDFE_{C-H}(HEH_2^*)$ = **–8.5 kcal mol^{-1}**

S7.2 Derivation of effective BDFE values ($BDFE_{eff}$) relevant to this work

Estimation of $BDFE_{eff}$ for HEH_2:

½ HEH_2 ⇌ ½ $HEH^{\bullet}$ + ½ $H^{\bullet}$	½ $BDFE_{C–H}(HEH_2)$ = 31.2 kcal mol^{-1}
½ $HEH^{\bullet}$ ⇌ ½ HE + ½ $H^{\bullet}$	½ $BDFE_{N–H}(HEH^{\bullet})$ = 20.3 kcal mol^{-1}
½ HEH_2 ⇌ ½ HE + $H^{\bullet}$	$BDFE_{eff}(HEH_2)$ = **51.4 kcal mol^{-1}**

Estimation of $BDFE_{eff}$ for $[HEH_2]$* as reductant and $[ColH]^+$ as acid:

HEH_2* ⇌ $HEH_2^{\bullet+}$ + e^-	23.06($E_{ox}(HEH_2$*)) = –62.3 kcal mol^{-1}
$[ColH]^+$ ⇌ Col + H^+	1.37(pK_a) = 20.6 kcal mol^{-1} (Ref 13)
$H^+ + e^-$ ⇌ Col + $H^{\bullet}$	C_G = 52.6 kcal mol^{-1}
HEH_2* + $[ColH]^+$ ⇌ $HEH_2^{\bullet+}$ + Col + $H^{\bullet}$	$BDFE_{eff}$ = **10.9 kcal mol^{-1}**

Estimation of $BDFE_{eff}$ for $[Ir^{II}]$ as reductant and $[ColH]^+$ as acid:

$[Ir^{II}]$ ⇌ $[Ir^{III}]^+$ + e^-	23.06($E_{ox}([Ir^{II}])$ = –43.8 kcal mol^{-1} (Ref 14)
$[ColH]^+$ ⇌ Col + H^+	1.37(pK_a) = 20.6 kcal mol^{-1} (Ref 13)
$H^+ + e^-$ ⇌ Col + $H^{\bullet}$	C_G = 52.6 kcal mol^{-1}
HEH_2* + $[ColH]^+$ ⇌ $HEH_2^{\bullet+}$ + Col + $H^{\bullet}$	$BDFE_{eff}$ = **29.3 kcal mol^{-1}**

S7.3 Estimation of overpotential for hydrogenation of N_2 with HEH_2 to NH_3

We derive the BDFE of H_2 in MeCN at 298 K explicitly here for clarity, using recently updated thermochemical values ():

$H_{2(g)} \rightleftharpoons 2\ H^+ + 2\ e^-$ $\quad 2\times23.06(E°(H^+/H_2)) = 2\times23.06(-0.028\ V) = -1.29$ kcal mol^{-1} (Ref 11)
$2\ H^+ + 2\ e^- \rightleftharpoons 2H^\bullet$ $\quad 2(C_G) = 105.2$ kcal mol^{-1}
$H_{2(g)} \rightleftharpoons 2H^\bullet$ $\quad$ BDFE(H_2) = **103.9 kcal mol^{-1}**

The overpotential $\Delta\Delta G_f(NH_3)$ for a source of hydrogen atom equivalents with a given $BDFE_{eff}$ is described by **eqn S1**:

$$\Delta\Delta G_f(NH_3) = 3(BDFE(H_2)/2 - BDFE_{eff}) \textbf{ (eqn S1)}$$

For the dark reaction, $\frac{1}{2}\ N_2 + \frac{3}{2}\ HEH_2 \rightleftharpoons NH_3 + \frac{3}{2}\ HE$:

$$\Delta\Delta G_f(NH_3) = 3(103.9/2 - 51.4) = \textbf{1.7 kcal mol}^{-1}$$

For the Ir-free reaction, in which $[HEH_2]$* is thought to be the strongest reductant accessed and $[ColH]^+$ serves as acid:

$$\Delta\Delta G_f(NH_3) = 3(103.9/2 - 10.9) = \textbf{123.2 kcal mol}^{-1}$$

For the Ir-photosensitized reaction, in which $[Ir^{II}]$ is thought to be the strongest reductant accessed and $[ColH]^+$ serves as acid:

$$\Delta\Delta G_f(NH_3) = 3(103.9/2 - 29.3) = \textbf{68.0 kcal mol}^{-1}$$

$\Delta G_f(NH_3)$ in MeCN at 298 K:

$\frac{1}{2}\ N_2 + \frac{3}{2}\ H_{2(g)} \rightleftharpoons NH_3$ $\quad \Delta G_f(NH_3) = -3\times23.06(E°(N_{2(g)}/NH_3)) = -3\times23.06(0.063\ V$ vs. $H_2)$[10]
$= \textbf{4.36 kcal mol}^{-1}$

With this value, we can also estimate the absolute driving force for hydrogenation of N_2 with HEH_2.

$\frac{1}{2}\ N_2 + \frac{3}{2}\ HEH_2 \rightleftharpoons NH_3 + \frac{3}{2}\ HE$ $\quad \Delta G_{rxn} = \Delta G_f(NH_3) - \Delta\Delta G_f(NH_3, HEH_2) = -4.4 - 1.7$ kcal mol^{-1}
$= \textbf{–6.1 kcal mol}^{-1}$

S8 NMR spectra:

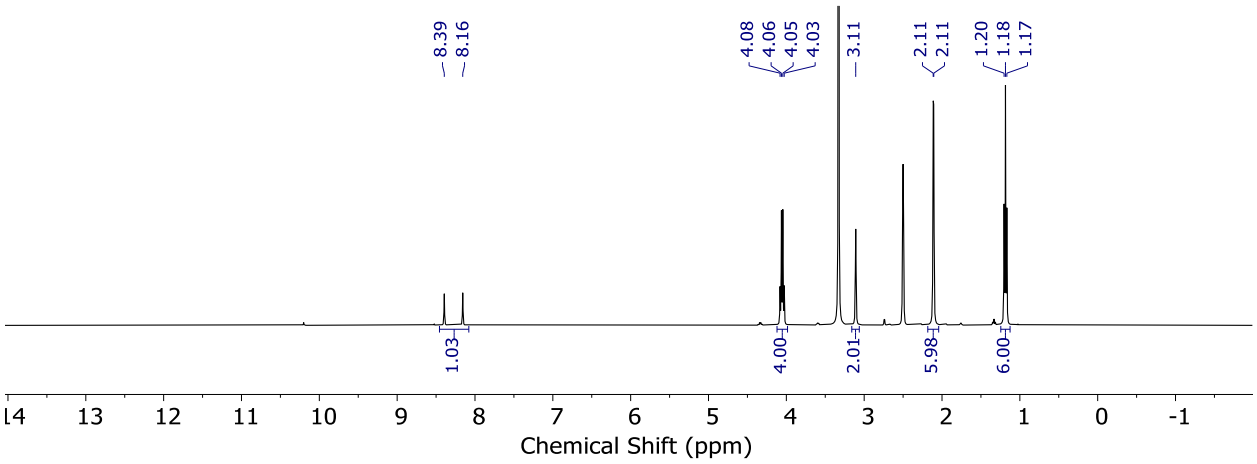

Figure S13. ^{1}H NMR (DMSO-d_6, 400 MHz) of ^{15}N-HEH$_2$.

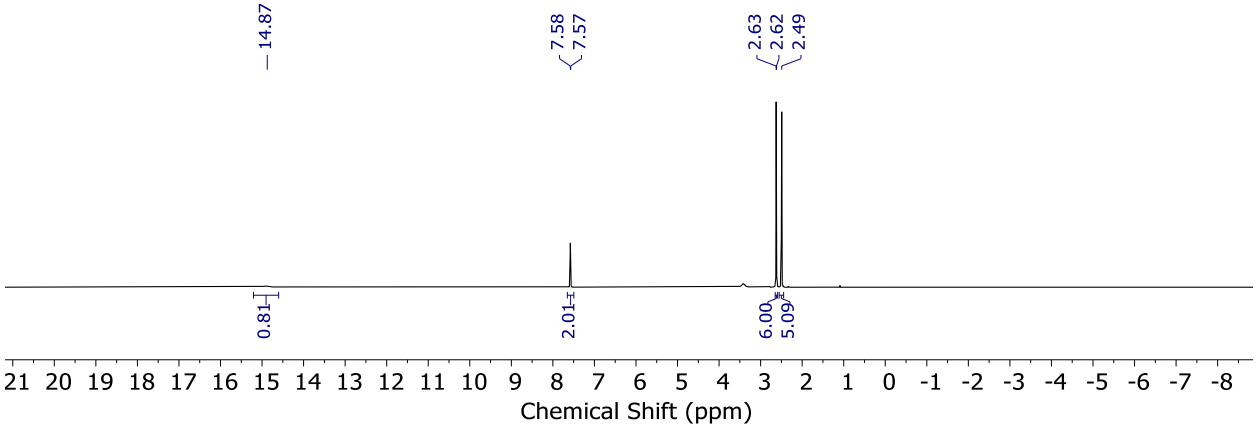

Figure S14. ^{1}H NMR (DMSO-d_6, 400 MHz) of ^{15}N-labelled [ColH]OTf.

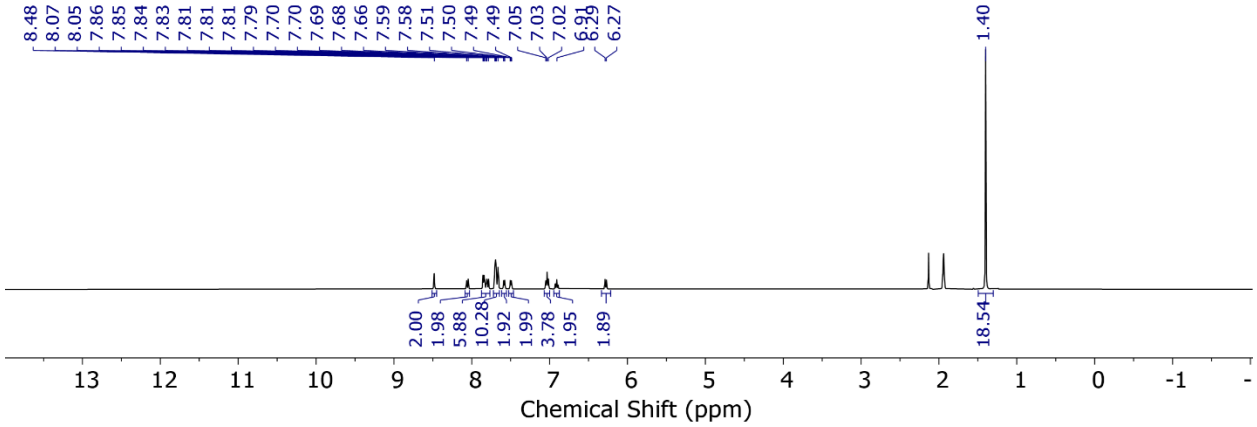

Figure S15. ^{1}H NMR (MeCN-d_3, 400 MHz) of [Ir]BAr$^{F}_4$.

References

1. B. E. Norcross, G. Clement, M. Weinstein, The Hantzsch pyridine synthesis: A factorial design experiment for the introductory organic laboratory. *J. Chem. Educ.* **46**, 694 (1969).

2. K. Arashiba, A. Eizawa, H. Tanaka, K. Nakajima, K. Yoshizawa, Y. Nishibayashi, Catalytic Nitrogen Fixation via Direct Cleavage of Nitrogen–Nitrogen Triple Bond of Molecular Dinitrogen under Ambient Reaction Conditions. *Bull. Chem. Soc. Jpn.* **90**, 1111–1118 (2017).

3. G.-B. Shen, Y.-H. Fu, X.-Q. Zhu, Thermodynamic Network Cards of Hantzsch Ester, Benzothiazoline, and Dihydrophenanthridine Releasing Two Hydrogen Atoms or Ions on 20 Elementary Steps. *J. Org. Chem.* **85**, 12535–12543 (2020).

4. T. J. Del Castillo, N. B. Thompson, J. C. Peters, A Synthetic Single-Site Fe Nitrogenase: High Turnover, Freeze-Quench ^{57}Fe Mössbauer Data, and a Hydride Resting State. *J. Am. Chem. Soc.* **138**, 5341–5350 (2016).

5. N. S. Golubev, S. N. Smirnov, P. Schah-Mohammedi, I. G. Shenderovich, G. S. Denisov, V. A. Gindin, H. H. Limbach, Study of acid-base interaction by means of low-temperature NMR spectra. Structure of salicylic acid complexes. *Russ. J. Gen. Chem.* **67**, 1082–1087 (1997).

6. L. Matesic, J. M. Locke, K. L. Vine, M. Ranson, J. B. Bremner, D. Skropeta, Synthesis and anti-leukaemic activity of pyrrolo[3,2,1-hi]indole-1,2-diones, pyrrolo[3,2,1-ij]quinoline-1,2-diones and other polycyclic isatin derivatives. *Tetrahedron* **68**, 6810–6819 (2012).

7. R. Brišar, F. Unglaube, D. Hollmann, H. Jiao, E. Mejía, Aerobic Oxidative Homo- and Cross-Coupling of Amines Catalyzed by Phenazine Radical Cations. *J. Org. Chem.* **83**, 13481–13490 (2018).

8. G. R. Fulmer, A. J. M. Miller, N. H. Sherden, H. E. Gottlieb, A. Nudelman, B. M. Stoltz, J. E. Bercaw, K. I. Goldberg, NMR Chemical Shifts of Trace Impurities: Common Laboratory Solvents, Organics, and Gases in Deuterated Solvents Relevant to the Organometallic Chemist. *Organometallics*. **29**, 2176–2179 (2010).

9. M. W. Weatherburn, Phenol-hypochlorite reaction for determination of ammonia. *Anal. Chem.* **39**, 971–974 (1967).

10. G. W. Watt, J. D. Chrisp, Spectrophotometric Method for Determination of Hydrazine. *Anal. Chem.* **24**, 2006–2008 (1952).

11. R. G. Agarwal, S. C. Coste, B. D. Groff, A. M. Heuer, H. Noh, G. A. Parada, C. F. Wise, E. M. Nichols, J. J. Warren, J. M. Mayer, Free Energies of Proton-Coupled Electron Transfer Reagents and Their Applications. *Chem. Rev.* **122**, 1–49 (2022).

12. J. Jung, J. Kim, G. Park, Y. You, E. J. Cho, Selective Debromination and α-Hydroxylation of α-Bromo Ketones Using Hantzsch Esters as Photoreductants. *Adv. Synth. Catal.* **358**, 74–80 (2016).

13. S. Tshepelevitsh, A. Kütt, M. Lõkov, I. Kaljurand, J. Saame, A. Heering, P. G. Plieger, R. Vianello, I. Leito, On the Basicity of Organic Bases in Different Media. *Eur. J. Org. Chem.* **2019**, 6735–6748 (2019).

14. J. D. Slinker, A. A. Gorodetsky, M. S. Lowry, J. Wang, S. Parker, R. Rohl, S. Bernhard, G. G. Malliaras, Efficient Yellow Electroluminescence from a Single Layer of a Cyclometalated Iridium Complex. *J. Am. Chem. Soc.* **126**, 2763–2767 (2004).